Impact of the sea surface temperature in the north-eastern tropical Atlantic on precipitation over Senegal

Mamadou Thiam[1,2], Ludivine Oruba[2], Gaelle de Coetlogon[2], Malick Wade[1], Bouya Diop[1], Abdou Karim Farota[1]

[1]Laboratoire des Sciences de l'Atmosphère et des Océans – Matériaux, Énergie et Dispositifs (LSAO-MED), Université Gaston Berger, Saint-Louis, Sénégal
[2]Laboratoire Atmosphère et Observations Spatiales (LATMOS), Sorbonne Université, Paris, France

Key Points:

- Wet summers in Senegal are preceded by La Niña events and warming in the Mediterranean but also by warming in the Northeastern Tropical Atlantic
- Moisture transport convergence within a stronger West African Westerly Jet (WAWJ) explains this increase in precipitation
- Feedback between the North Tropical Atlantic surface temperature and atmospheric pressure is proposed to explain this WAWJ acceleration

Corresponding author: Mamadou Thiam, thiam.mamadou9@ugb.edu.fr

Abstract

This study examines 40 years of monthly precipitation data in Senegal (1979-2018) using CRU observations and ERA5 reanalyses, aiming to understand the influence of oceanic and atmospheric factors on Senegal's precipitation in July, August and September (JAS). The variability of Senegal's precipitation is first compared with that of the broader Sahel region: although they share a significant portion of their variance, Senegal appears more closely related to the Northeastern Tropical Atlantic (NETA) Sea Surface Temperature (SST). A detailed examination of this region reveals that Senegal's increased precipitation is linked to the northward shift of the InterTropical Convergence Zone (ITCZ), consistent with numerous previous studies. Over the continent, this shift corresponds to a northward shift of the African Easterly Jet (AEJ) and, consequently, the Mesoscale Convective Systems responsible for most precipitation. It seems primarily driven by the northward shift of the Heat Low. Over the ocean just west of Senegal, there is a comparable shift of the AEJ, accompanied by an increase in low-level moisture transport convergence within the West African Westerly Jet (WAWJ) which explains the majority of the increase in JAS precipitation in Senegal. This phenomenon is triggered by a negative pressure anomaly in the NETA, located above a positive Sea Surface Temperature (SST) anomaly: we suggest that the latter is the origin of the former, forming a feedback mechanism that potentially significantly influences Senegal's precipitation. The mechanism involves a geostrophic adjustment of the WAWJ to the southern gradients of the SST anomaly. Further investigations utilizing daily data or regional atmospheric models are necessary to validate the role of NETA SST feedback on Senegal's precipitation, with potential benefits for enhancing seasonal forecasting capabilities.

Plain Language

This study, spanning 40 years of monthly precipitation data in Senegal, explores the intricate relationship between oceanic and atmospheric factors shaping precipitation patterns from July to September. The increased summertime precipitation in the Western Sahel is primarily of continental origin, associated with the northward shift of mesoscale convective systems linked to lower pressure in the Sahara. However, over the ocean west of Senegal, there is also an increase in inland moisture transport that explains a significant part of the intensified precipitation from July to September in Senegal. This transport is reinforced by a low-pressure system over the ocean, potentially caused by warmer sea surface temperatures between 10°N and 20°N off West Africa. This close connection between Senegal's precipitation and ocean surface temperature in the Northeastern Tropical Atlantic could help enhance crucial seasonal forecasts for agricultural planning, the economy, and food security in West Africa.

1 Introduction

The study of Sahel's rainfall variability is crucial due to its vulnerability to climate change. Accurate forecasts are vital for managing water resources, agriculture, and health (Sultan et al., 2005; Grace & Davenport, 2021). This semi-arid region, experiences most of its precipitation from July to September (JAS). During this period, a zonal rain belt spans from approximately 5°N to 15°N across West Africa, shifting southward the rest of the year (Parker & Diop-Kane, 2017). The summer rains are primarily attributed to mesoscale convective systems (MCSs), with up to 95% originating above the eastern highlands and crossing East to West Africa within one or two days (Nicholson, 2013). These systems form due to the African Easterly Jet (AEJ)'s presence in the mid-troposphere, particularly its southern half, with strong horizontal vorticity facilitating barotropic and baroclinic instabilities (Parker & Diop-Kane, 2017).

This zonal band of precipitation experiences strong year-to-year and even decadal variations between 10°N and 15°N. For instance, an exceptionally severe drought occurred in the 1980s (Le Barbé & Lebel, 1997). Various mechanisms have been identified to explain this extensive variability, including the land-atmosphere-ocean system and changes in atmospheric circulation patterns and weather systems behavior in West Africa during the rainy season (Zeng et al., 1999; Nicholson & Palao, 1993; Vizy & Cook, 2001). Nevertheless, numerous studies highlight the pivotal role of global sea surface temperature (SST) such as the Indian Ocean warming (Hagos & Cook, 2008), which influences the African monsoon through atmospheric teleconnections through modifications in Walker cells intensity, or equatorial atmospheric Kelvin and Rossby waves (Wang, 2019). Strong correlations have indeed been observed between Sahel precipitation and remote SST at interannual timescales in the Pacific equatorial region (Janicot et al., 2001; Joly & Voldoire, 2009; Diatta & Fink, 2014; Gomara et al., 2017), in the Mediterranean Sea (Rowell, 2003; Jung et al., 2006; Polo et al., 2008; Fontaine et al., 2009; Diakhate et al., 2019; Worou et al., 2020), or in the Indian Ocean (Bader & Latif, 2003; Biasutti et al., 2008; Mohino et al., 2011; Caminade & Terray, 2010).

Sahel rainfall variability may also be influenced by coupled regional dynamics in the Tropical Atlantic (Camberlin et al., 2001; Polo et al., 2008). At interannual timescales, the SST in the Gulf of Guinea is influenced by an equatorial ocean-atmosphere coupled mode known as the "zonal mode" or Atlantic Niño (Zebiak, 1993; Cabos et al., 2019), subsequently affecting precipitation along the Guinea Coast (Meynadier et al., 2016; Polo et al., 2008; de Coëtlogon et al., 2010, 2014) and, seemingly, in the Sahel (Caniaux et al., 2011; Steinig et al., 2018; Janicot et al., 1998; Vizy & Cook, 2001; Losada et al., 2010). Regarding the North Tropical Atlantic, Mo et al. (2001) and Ward (1998) suggested that NETA SST does not significantly influence West African rainfall. Using a general circulation model, Vizy and Cook (2001) also concluded that precipitation over West Africa is generally insensitive to NETA SST anomalies. In the other hand, Camberlin and Diop (1999) found that precipitation in Senegal is more sensitive to climatic anomalies in the northern Tropical Atlantic than in the rest of the Sahel over the period 1960-1990. Moreover, Fall et al. (2006) found that precipitation over Senegal is well correlated with North Tropical Atlantic SST from January to May. The role of NETA SST in relation to Sahel precipitation remains therefore unclear, especially for western Sahel. However, Sahel precipitation in summer is strongly linked to the latitude of the intertropical convergence zone (Camberlin et al., 2001; Nicholson, 2013), and the latter could be tied to the zonal band of maximum SST in the Tropical Atlantic (Diakhaté et al., 2018): when the SST in the Northeastern Tropical Atlantic (NETA) is warmer than those further south, the ITCZ migrates northward, leading to positive rainfall anomalies observed in the Sahel (Xie & Carton, 2004; Gu & Adler, 2009; Gu, 2010; Janicot et al., 2001; Biasutti et al., 2008). It therefore appears important to clarify whether NETA SST has an impact on Sahel precipitation, carefully distinguishing between Senegal (Western Sahel) and Central Sahel.

The primary objective of this paper is to build a robust index of Senegal precipitation for monitoring its variability based on observations. It then briefly revisits teleconnections between global SST and precipitation on interannual timescales with a particular focus on Senegal specifically, in contrast to the broader Sahel region as commonly done in previous research. Subsequently, we delve deeper into the NETA signatures of SST, Sea Level Pressure (or SLP), wind fields, and low-level moisture transport anomalies: we discuss their influence on Senegal's precipitation patterns and consider the potentiel role of a regional SST feedback mechanism on precipitation in West Africa. The paper is divided as follows: Section 2 describes the data and the methods, Section 3 presents the building of the index, Section 4 discusses the signals found in global SST, Section 5 focuses on the NETA SST and near-surface dynamics, Section 6 discusses the moisture transport and precipitation, Section 7 proposes a mechanism for the SST influence on the WAWJ, and Section 8 concludes the study.

2 Data and methods

2.1 Data

The present study relies on the Climatic Research Unit (CRU) Time-series (TS). The CRU TS dataset was originally created and subsequently updated by the UK Natural Environment Research Council (NERC) and the US Department of Energy. In this paper, we utilized Version 4.03 of the CRU TS dataset, which spans the period from 1901 to 2018 at a high resolution of $0.5^\circ \times 0.5^\circ$. Monthly averaged precipitation data for the mainland, covering the period from 1979 to 2018, were acquired from various weather services and other sources.

CMWF Reanalysis v5 (ERA5) data are employed in this study to monitor the atmospheric dynamics associated with Senegal precipitation fluctuations. ERA5 is produced by the Copernicus Climate Change Service (C3S) and incorporates data assimilation, combining model data with observations from worldwide sources. It provides estimates for numerous atmospheric, terrestrial, and oceanic climate variables from 1979 to the present day, with a horizontal grid resolution of $0.25^o \times 0.25^o$ and 37 vertical levels ranging from 1000 to 1 hPa and we also use monthly average data. Global SST data from ERA5 are used to identify global teleconnections with precipitation. These SST data are based on the Hadley Centre Sea Ice and Sea Surface Temperature dataset version 2 (HadISST2) from 1979 to August 2007 and the Office Operational Sea Surface Temperature and Sea Ice Analysis (OSTIA) daily product from September 2007 to the present. These SST datasets closely align with the Reynolds observation product (Yang et al., 2021).

The atmospheric parameters used in this study are SLP, zonal (u) and meridional wind (v) at 10 meters above the surface, and at the available pressure levels in ERA5. Additionally, geopotential height (Z) and specific humidity (q) are also used. Wind speed ($\sqrt{u^2 + v^2}$) is treated as an additional parameter: we calculate its monthly seasonal anomalies separately from the zonal and meridional components. Linear regressions of wind speed anomalies hence indicate whether the wind anomalies correspond to a weaker (negative anomalies) or stronger (positive) wind speed in comparison to the average.

2.2 Linear statistical tools

The calculation of monthly seasonal anomalies is conducted over the 40-year period from 1979 to 2018 for all parameters. Anomalies are determined by subtracting the seasonal cycle, computed by averaging the values for each month over the 1979-2018 period. Additionally, to remove long-term periodicities (decadal and beyond), a quadratic trend computed over the 480 monthly anomalies is removed from these anomalies in all parameters.

Empirical Orthogonal Function (EOF) decomposition are performed in both the CRU and ERA5 precipitation anomalies in JAS over Senegal in section 3. The Principal Components (PCs) represent the eigenvectors of the estimated covariance matrix. Following the approach outlined in Von Storch and Zwiers (1999), the spatial patterns, also known as EOFs, correspond to the linear regression of the JAS anomalies on the PCs as described just below.

Given an independent, identically distributed sample of random parameters X_i and Y_i for $i = 1$ to $n = 120$ (i.e. 40 years times 3 months), the correlation is computed

with the following maximum likelihood estimator:

$$\hat{R} = \frac{\sum_{i=1}^{n}(X_i - \overline{X})(Y_i - \overline{Y})}{\sqrt{\left(\sum_{i=1}^{n}(X_i - \overline{X})^2\right)\left(\sum_{i=1}^{n}(Y_i - \overline{Y})^2\right)}} \tag{1}$$

Here, $\overline{X} = \frac{1}{n}\sum_{i=1}^{n} X_i$ and $\overline{Y} = \frac{1}{n}\sum_{i=1}^{n} Y_i$ are estimators of the variables means. Subsequently, we apply the least squares estimate of the slope of the simple linear regression, as described in Von Storch and Zwiers (1999):

$$\hat{a} = \frac{\sum_{i=1}^{n}(X_i - \bar{X})(Y_i - \bar{Y})}{\sqrt{\sum_{i=1}^{n}(X_i - \bar{X})^2}} \tag{2}$$

The resulting $\hat{a}$ field represents the variation of Y associated with a fluctuation of one standard deviation of X. For example, if (X_i) represents the normalized PC1CRU index, and (Y_i) represents the SST, $\hat{a}$ indicates the change in SST anomalies (in °C) associated with a one-standard deviation increase in the precipitation index. This resulting field is typically referred to as the SST anomaly obtained from the regression of SST on the precipitation index. Note that all descriptions in this study pertain to positive values of this index, reflecting anomalies associated with higher-than-average JAS precipitation in Senegal. However, we could have chosen to describe opposite anomalies (i.e., related to a dry summer) without altering the interpretation of our results.

Moreover, we employ the unbiased estimator $\sigma(X) = \sqrt{\frac{1}{n-1}\sum_{i=1}^{n} X_i^2}$ to calculate the standard deviation of a random variable X based on a sample of n values. By considering X_i as the July anomalies, Y_i as the August anomalies and Z_i as the September anomalies, we proceed to estimate the typical interannual anomaly (i.e., averaged over the entire JAS season) as follows:

$$\sigma_{interannual} = \sqrt{\frac{1}{N-1}\sum_{i=1}^{N} {XYZ_i}^2}$$

where $N = 40$ years and $XYZ_i = \frac{X_i + Y_i + Z_i}{3}$ is the yearly anomaly in JAS, whereas the intraseasonal signal, representing the typical monthly anomaly within each JAS season (independently of the variations between the different JAS averages), is estimated as follows:

$$\sigma_{\text{intraseasonal}} = \sqrt{\frac{1}{3N-1}\sum_{i=1}^{N}\left(X_i - XYZ_i\right)^2 + \left(Y_i - XYZ_i\right)^2 + \left(Z_i - XYZ_i\right)^2}$$

Finally, to distinguish meaningful correlations from chance occurrences, a p-value of 0.05 (95% confidence level) is chosen, indicating a one-in-twenty probability that a correlation exceeds the threshold by pure coincidence. The determination of this threshold depends on the number of independent data points in the time series. In this study, we allocate one degree of freedom per month, having verified that the three monthly data points per year are uncorrelated in the reference time series (PC1CRU, defined in section 3). The correlation between July and August anomalies is indeed 0.16, and 0.21 between August and September, both well below the significant correlation threshold of

0.31 with 40 degrees of freedom, ensuring the independence of the 120 monthly values. With a degree of freedom of 120, the 95% confidence level for correlation yields the threshold of 0.18: only linear regression values with correlations exceeding this value are depicted in the following figures or discussed in the text as either "positive anomalies" or "negative anomalies."

2.3 Moisture transport and divergence

We calculate moisture transport using specific humidity (q) and horizontal winds $\mathbf{U} = (u, v)$. At each pressure level, moisture transport is computed as $q.\mathbf{U}$. To integrate this calculation from p_b to p_t, we apply a weight factor to each pressure level, dP/g. This factor corresponds to the mass per unit area of the respective pressure interval (i.e., ρdz, where ρ represents the air density) using the hydrostatic approximation ($dp = -\rho g dz$):

$$\mathbf{HT} = \frac{1}{g} \int_{p_b}^{p_t} q.\mathbf{U}.dp \tag{3}$$

The result gives the integrated moisture transport between p_b and p_t in $kg.m^{-1}.s^{-1}$

The horizontal divergence of the moisture transport is calculated at each pressure level by using a centered scheme on the zonal and meridional components HT_x and HT_y as follows:

$$\nabla \cdot \mathbf{HT}(i,j) \;=\; \frac{HT_x(i+1,j) - HT_x(i-1,j)}{2\,\delta x} + \frac{HT_y(i,j+1) - HT_y(i,j-1)}{2\,\delta y} \tag{4}$$

where i and j are the indices of the gridpoints, and δx and δy are the zonal and meridional lengths of the gridpoints.

3 JAS precipitation index for Senegal

The highest rainfall in Senegal is observed during July, August and September (JAS), with the peak occurring in August. In the other quarters (not shown), it decreases to approximately 10-30% of this peak, consistent with prior research (Rowell et al., 1995; Sultan & Janicot, 2000; Grist & Nicholson, 2001; Lebel et al., 2003; Fall et al., 2006). JAS averages are presented for both the CRU observation-based data product (Figure 1a) and ERA5 reanalyses (Figure 1b). Both datasets exhibit a clear zonal symmetry, with values increasing from north to south (Figure 1a, b), consistent with previous studies (Camberlin et al., 2001; Moron et al., 2006; Rust et al., 2013). The maximum precipitation occurs in the southern region, ranging from 8 to 12 mm/day in the southwest, while it remains below 3 mm/day in the northern part. A bias of about 1-2 mm/day is noted in ERA5 reanalyses, with a maximum of 2-3 mm/day along the western coast and in the southeast (Figure 1e).

We first examine the interannual variability: monthly JAS anomalies were averaged for each year, resulting in 40 annual anomalies from 1979 to 2018, and their standard deviation $\sigma_{interannual}$ (see section 2.2) plotted in Figures 1c and d. Like the average, they exhibit a zonal pattern with values decreasing from south to north: regions with higher average precipitation also display larger interannual variability. The standard deviation appears slightly smaller in ERA5 than in observations (by about 0.5 mm/day); however, the standard deviation of this bias (obtained by computing the standard deviation of the time series differences between observations and ERA5) is comparable to or smaller than the JAS precipitation standard deviation (Figure 1f), accounting for approximately only 10-25% of the mean value. Consequently, ERA5 data reasonably capture the interannual variability of Senegal precipitation in JAS. Nevertheless, averaging values in JAS to a single value per year results in the loss of the intraseasonal signal contained within these three summer months. Since we aim to identify related signals in SST,

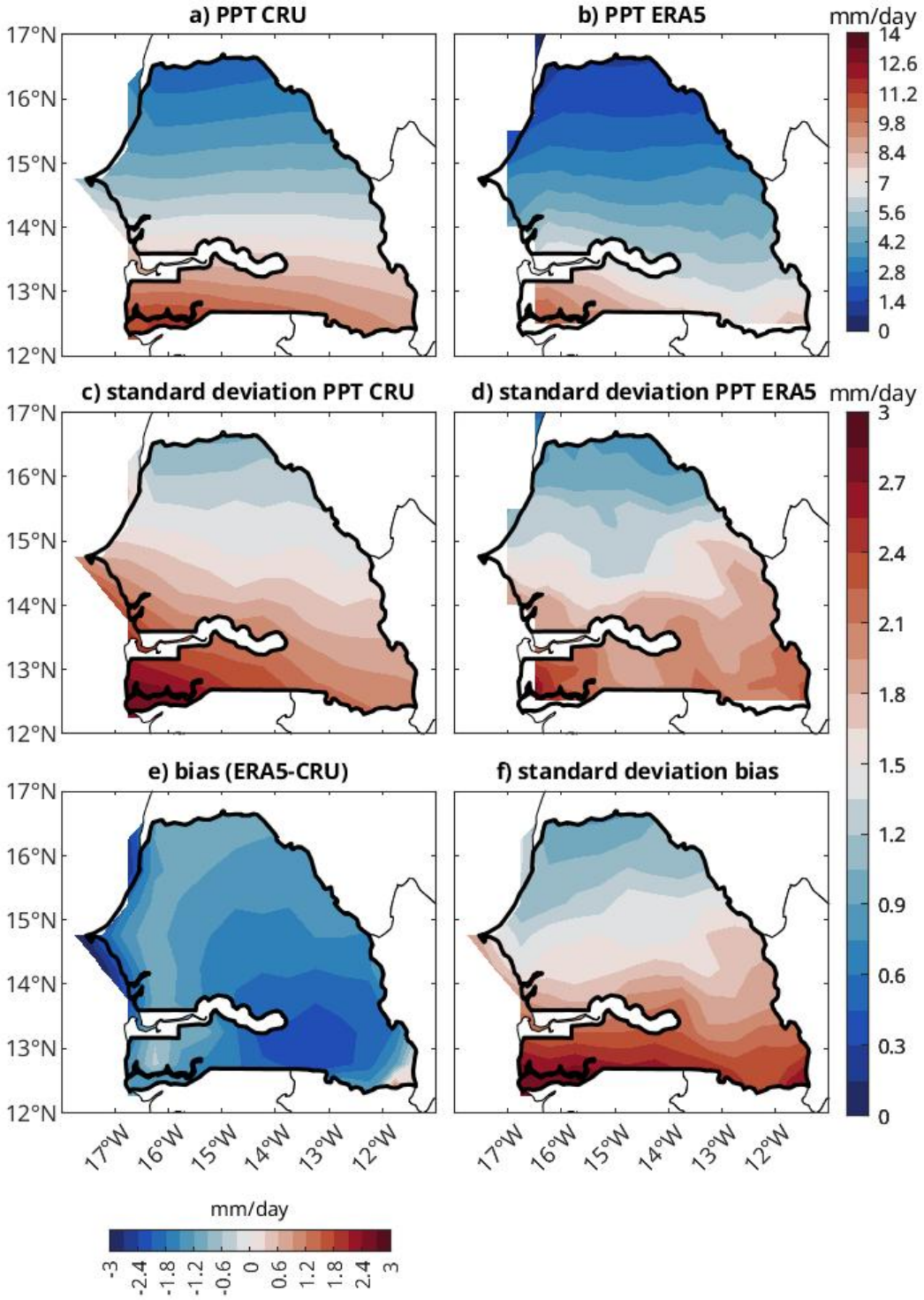

Figure 1. JAS 1979-2018 precipitation (PPT) in Senegal (mm/day): a. CRU observations, b. ERA5 reanalyses, c. standard deviation of CRU anomalies, d. standard deviation of ERA5 anomalies, e. mean bias between CRU observations and ERA5 reanalyses, f. standard deviation of the bias.

which has proven challenging due to the contrasting findings in previous studies, it is crucial to preserve the maximum signals. Therefore, we retain each individual July, August, and September anomaly throughout the remainder of the paper, including in the EOF decomposition.

The resulting first EOF of the CRU data (EOF1) accounts for 66.1% of the total variance (Figure 2a). Interestingly, the associated principal component (or PC1) time series yields a $\sigma_{intraseasonal}$ of 0.75, larger than the $\sigma_{interannual}$ of 0.66. This indicates that retaining three summer monthly values per year significantly enhances the representation of the intraseasonal (or intermonthly) variability in our analysis. The ERA5 EOF1 accounts for 48.5% of the total variance (Figure 2b). EOF1 are very similar in ERA5 and CRU: they both exhibit a monopolar structure (i.e. with values of the same sign all over Senegal) of the precipitation anomalies. With zonal symmetry, an increase in the anomaly amplitude is observed from north to south, logically reflecting the standard deviation (Figure 1c,d): it is maximum in the southwest of Senegal (in Casamance), with more than 0.1 mm/day in CRU mode, and about half of that in ERA5 mode. The time series associated with EOF1 (or PC1) for CRU and ERA5 (Figure 2c) both exhibit strong interannual and intraseasonal monthly variability in precipitation. Their correlation (0.71) is highly significant, and they also demonstrate substantial covariability within the three-month summer periods, with common extreme months (e.g., August 1984, September 1986, July 1997, July 2002, September 2010, etc.).

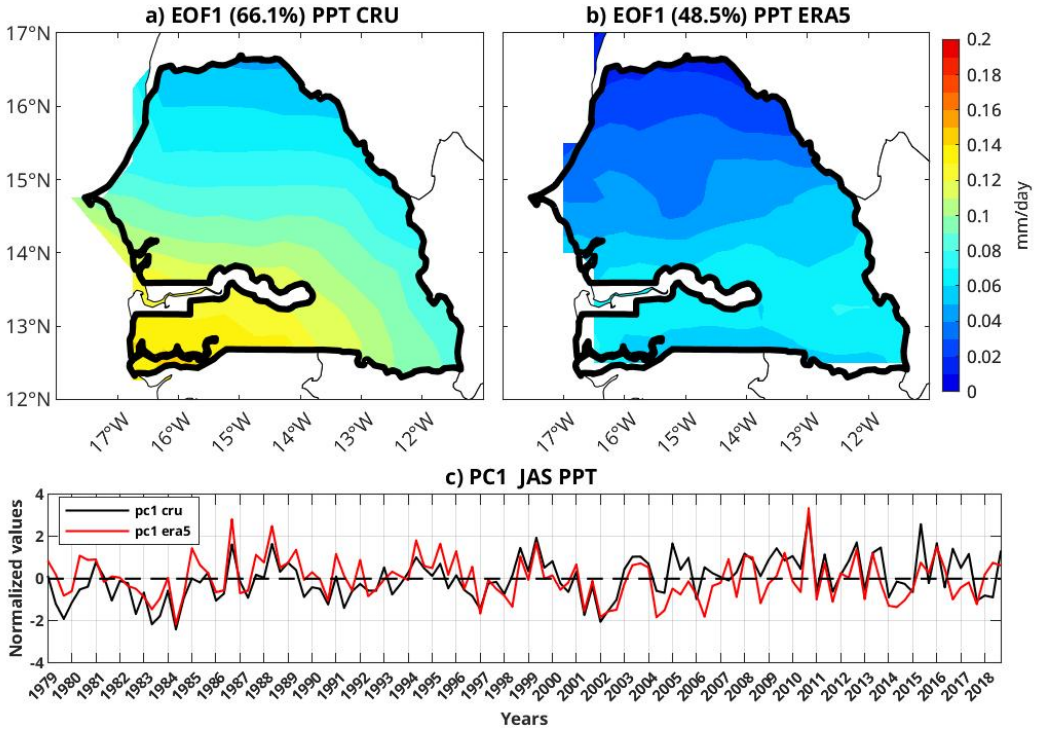

Figure 2. JAS 1979-2018, principal mode of variability (EOF1) for precipitation (PPT) anomalies (mm/day): a. CRU observations, b. ERA5 reanalyses and c. corresponding time series (black contours for CRU, red contours for ERA5).

The JAS mean and EOF1 precipitation for the entire Sahel region in both CRU and ERA5 datasets are not reproduced here but only in the annex (additional Figures A2 and A3), as they align with the findings of numerous previous studies, such as Quagraine et al. (2020). They exhibit similar zonal patterns, particularly covering the Senegal re-

gion, with maximum anomalies located in the west in both datasets. Although the Sahel's first mode explains approximately 33% of the variance in ERA5 and slightly over 40% in CRU observations (see Table A1), both Senegal's and Sahel's modes show a high degree of correlation in both datasets, indicating shared interannual / summer monthly intraseasonal variance of more than 50% in CRU and ERA5 (see Figure A3c).

In summary, we observe that ERA5 reanalyses effectively capture months of extreme precipitation in JAS, both at regional and local scales. These findings align with the conclusions of Quagraine et al. (2020). They are also in agreement with the work of Fall et al. (2006) and Wade et al. (2015), who identified a moderate but significant correlation between seasonal rainfall in Senegal and the rest of West Africa. While precipitation patterns are generally consistent across much of the Sahel, they exhibit slight variations in the western region near the Atlantic (primarily Senegal) compared to the continental sector (Nicholson & Palao, 1993). However, when performing an EOF decomposition over the entire West Africa region - not just the Sahel - Fall et al. (2006) found that Senegal's precipitation is more correlated with the second mode of variability of precipitation across West Africa than with the first mode, but this could only highlight the strong dependence of interannual variability modes on the selected region for analysis. Focusing on Senegal's modes, the second mode in the CRU data accounts for approximately 10% of the total variance (see additional Figure A1 and Table A1), whereas the first mode explains two-thirds of the variance: consequently, in the subsequent analysis, we use CRU's PC1 for JAS as a summer monthly interannual / intraseasonal index of JAS precipitation in Senegal. This index is hereafter referred to as PC1CRU. Lastly, while ERA5 precipitation does not perfectly match CRU observations, they do share a significant portion of their variance, indicating that the atmospheric dynamics in ERA5 are relevant for identifying the mechanisms leading to increased precipitation in Senegal.

4 Global SST anomalies

This section explores linear regressions of global SST anomalies on a reference index. First, we use the index characterizing precipitation variability across the entire Sahel in observations (plotted in additional Figure A3c, black). Following that, we compare these findings with the results obtained using the precipitation index specific to Senegal (PC1CRU). We present SST anomalies during the three summer months (JAS) and also the preceding months: the term 'lag -1' refers to the correlation between PC1CRU in JAS and SST anomalies with a 1-month lag (i.e., in JJA); 'lag -2' indicates a 2-month lag (MJJ), and so forth.

A wetter-than-average summer in Sahel is clearly associated with a La Niña-like signal in the eastern equatorial Pacific (red box, 170-80°W, 5°S-5°N), characterized by negative SST anomalies, reaching more than -0.4°C at lag -5 (Figure 3). This signal reflects an anticorrelation between SST anomalies in the eastern equatorial Pacific and PC1CRU Sahel. It begins to show significance in spring (lag -5, or FMA), but the maximum anticorrelation is observed at lag -3 (in AMJ): SST in this region between April and June would have a significant impact on Sahel's summer rainfall, as discussed in numerous previous studies (Folland et al., 1986; Janicot et al., 2001; Giannini et al., 2003; Joly & Voldoire, 2009; Rodríguez-Fonseca et al., 2011; Diatta & Fink, 2014; Gomara et al., 2017; Diakhaté et al., 2020): during an El Niño event (warm waters in the equatorial Pacific), warm Pacific waters trigger a Kelvin atmospheric wave associated with increased subsidence and reduced precipitation in West Africa (Semazzi et al., 1988; Moron & Ward, 1998; Rowell, 2001; Mohino et al., 2011). Joly and Voldoire (2009) suggested that the inverse mechanism is involved during a La Niña event, leading to increased monsoon rainfall in West Africa.

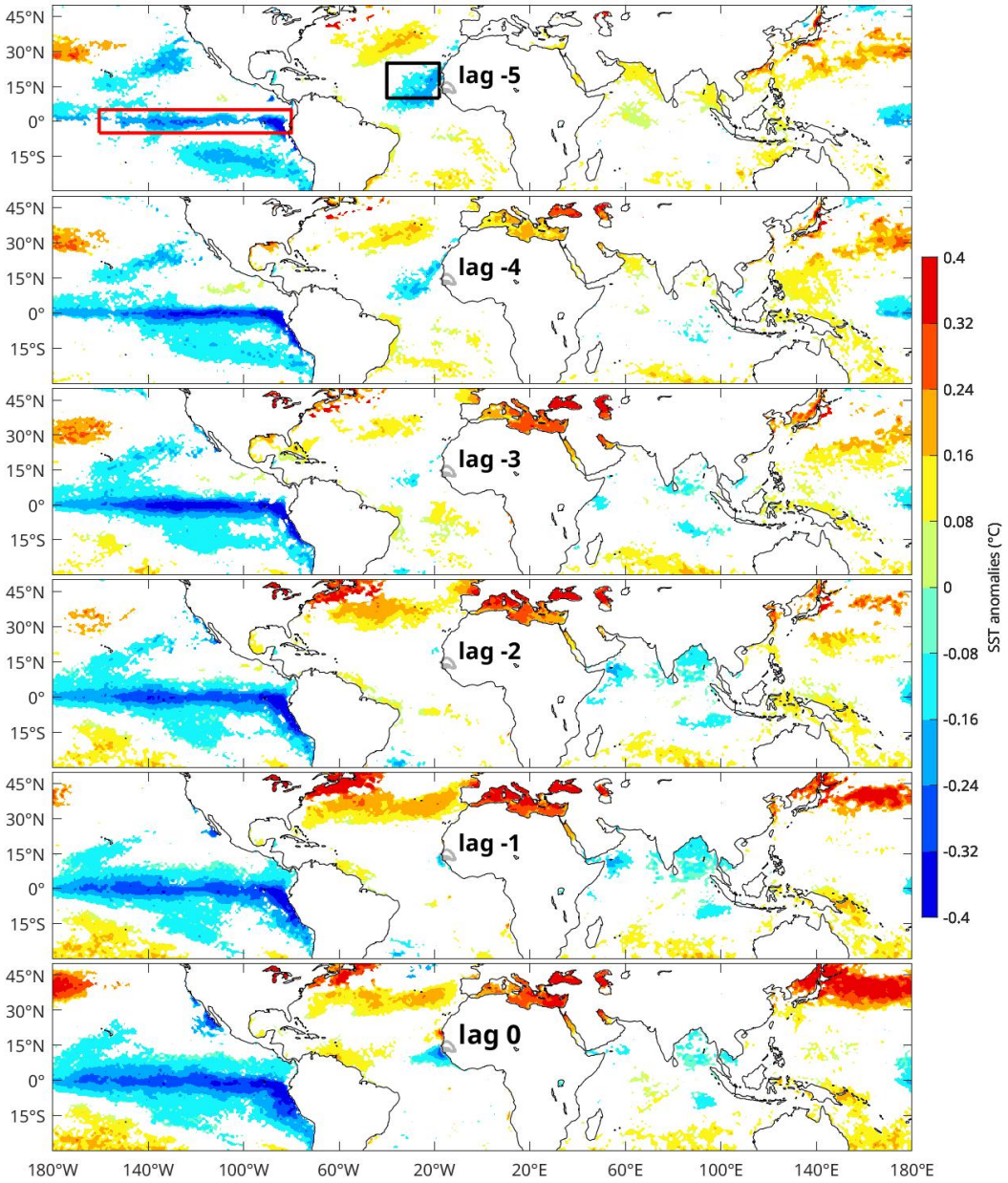

Figure 3. Linear regression of SST anomalies on PC1CRU Sahel (^oC) from lags -5 to 0 (indicating that SST precedes PC1CRU Sahel by 5 to 0 months). Only values significant at the 95% confidence level are plotted. The red box outlines the eastern equatorial Pacific (180°W-80°W, 5°S-5°N). The black box frames the Northeastern Tropical Atlantic (40°W-17°W, 10°N-25°N).

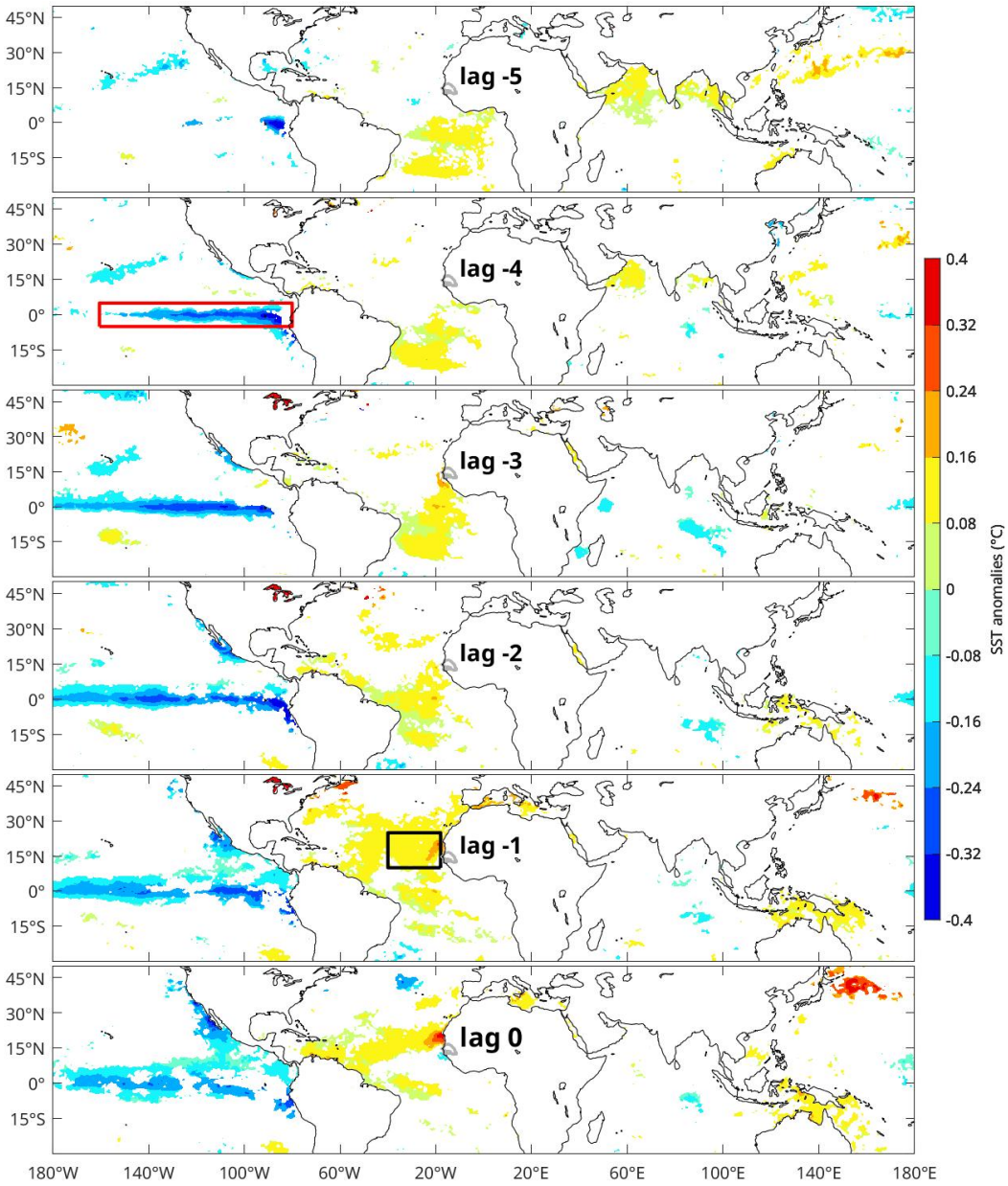

Figure 4. Identical to Figure 3 but for PC1CRU Senegal.

Strong significant positive SST anomalies in the Mediterranean precede a wetter-than-average summer in Sahel in the preceding months (Figure 3). This finding aligns with previous studies suggesting that increased SST leads to more rainfall through the supply of moisture over the Sahel, impacting Sahel precipitation (Rowell, 2003; Polo et al., 2008; Fontaine et al., 2009; Diakhate et al., 2019; Worou et al., 2020; Polo et al., 2008; Gaetani et al., 2010; Mohino et al., 2011; Gomara et al., 2017; Diakhate et al., 2019; Worou et al., 2020). Notably, Jung et al. (2006) identified a significant increase in Sahel rainfall following the 2003 Mediterranean heat episode. Very strong correlations are also found in the northern Atlantic, with anomalies exceeding 0.4° in the Gulf Stream region north of 30°N (Wang et al., 2012; Y. Liu et al., 2014; Monerie et al., 2020) or in the northwestern Pacific: Northern Hemisphere extratropical warming indeed induces a significant increase in Sahel rainfall through the modification of the large-scale meridional heat distribution, according to Park et al. (2015) or Suárez-Moreno et al. (2018).

Other significant signals are found in the Indian Ocean between lags -3 and -1, also highlighted in previous studies for the post-1970 period (Mohino et al., 2011; Fontaine et al., 2011). Although these signals appear relatively weak, they could nonetheless impact precipitation in the Sahel, as suggested in several studies (Bader & Latif, 2003; Biasutti et al., 2008; Mohino et al., 2011; Caminade & Terray, 2010). Hardly significant but large warm anomalies are found in the western tropical Pacific in the preceding months, likely as a continuation of the La Niña signal (Figure 3). However, no particular signal is found in the equatorial and subtropical South Atlantic. A signal corresponding to the 'Atlantic Niño' in the eastern equatorial Atlantic is observed, as in Dommenget and Latif (2000), but approximately one year before the start of the rainy season, at lags -10 and -9 (not shown).

In the linear regression on PC1CRU Senegal, the vast majority of the signals identified with PC1CRU Sahel are once again present but with weaker correlations and much less significant amplitudes (Figure 4). For example, the 'La Niña' signal in the eastern equatorial Pacific reaches up hardly -0.3°C at lag -3. The warm signal in the Mediterranean Sea is also significantly weaker and not observed until lag -1. On the other hand, a warm signal is found at lag -5 (FMA) in the equatorial Atlantic, disappearing by lag -1 (in JJA), and a warm anomaly appears around 15-20°S from lag -5 with a peak at lag -4: Camberlin and Diop (1999) and Fall et al. (2006) have also found this predictive power of the South Subtropical Atlantic on Senegal precipitation with approximately a 5-month lead time. Moreover, significant differences are observed in the NETA (black box, 40°-20°W, 5°-25°N), off the coast of Senegal and Mauritania: a positive anomaly of 0.2 to 0.3°C is observed in phase with and one month before heavy rainfall in Senegal (lags 0 and -1), where a negative anomaly was found instead in the regression on the Sahel index (Figure 3).

These results indicate that despite the high correlation observed between the two principal modes of precipitation, one obtained over the entire Sahel and the other specifically over Senegal, the latter appears to be less affected by remote SST anomalies commonly discussed in the literature. Instead, it is more influenced by regional SST in the NETA region as well as the South Tropical Atlantic. The latter aspect is beyond the scope of the present study. However, in the following sections, we examine in more detail the oceanic and atmospheric signals linked to Senegal's precipitation in the NETA region.

5 Anomalies of SST and near-surface atmospheric circulation in the Northeastern Tropical Atlantic

The JAS averages of SLP, SST, and surface winds from ERA5 reanalyses for the period 1979-2018 are shown in Figure 5. Over the continent, the primary characteristic of SLP is the "Heat Low" (Lavaysse et al., 2009), with values below 1010 hPa between 15°N and 30°N (Figure 5a, black contours). Further west and slightly northward over the

ocean, there is a maximum SLP in the Azores region, around 35°N. The significant pressure gradient between these two regions results in very strong northeasterlies over the ocean along the coast, and northerlies over the Western Sahara and southern Morocco (Figure 5b). In response, the signature of a coastal upwelling can be observed north of 20°N off Cap Blanc (the border between Mauritania and Western Sahara), with SST values decreasing to as low as 20-22°C (Figure 5a). Furthermore, north of 15°N, SST is warmer in the west than in the east: this is likely explained by the fact that, on a seasonal scale, SST is primarily balanced between solar heating on one hand and cooling through latent heat fluxes on the other hand (Foltz & McPhaden, 2006), with surface winds being stronger in the east compared to the west.

South / southeast trade winds are found south of 5°N (Figure 5b). East of 10-15°W, they turn north/northeastward while bringing moisture to West Africa ("monsoon flow"). Further west, over the ocean, they converge with the northeast trade winds between 5°N and 15°N, defining the Intertropical Convergence Zone (ITCZ) where SST is maximum. The convergence of surface winds and maximum SST are indeed closely linked in the tropics (Fontaine & Janicot, 1996; Xie & Carton, 2004). For instance, Diakhaté et al. (2018) suggested that SST gradients significantly influence pressure gradients along the edges of the ITCZ in the Atlantic Ocean. Following the mechanism of Lindzen and Nigam (1987), a SST gradient tends to induce an opposite gradient in SLP just above through turbulent heat fluxes and hydrostatic adjustment. Consequently, surface winds tend to converge toward the center of a warm tropical SST region, favoring weak surface winds and deep atmospheric convection in the core of the ITCZ. However, east of 30°W, these winds turn eastward under the influence of the Heat Low and its extension over the ocean, forming the WAWJ (highlighted in red frame), which blows from the Atlantic towards the continent around 10°N (Grodsky, 2003; Pu & Cook, 2010). This low-level jet, observed below 800 hPa (Bonner, 1968; Stensrud, 1996), is known to be a significant source of moisture for the West African Monsoon in boreal summer (Cadet & Nnoli, 1987; Grams et al., 2010; Thorncroft et al., 2011; Pu & Cook, 2012; Lélé et al., 2015; W. Liu et al., 2020). The moisture transport into West Africa, and consequently precipitation, is thus potentially influenced by NETA SST through its impact on the WAWJ.

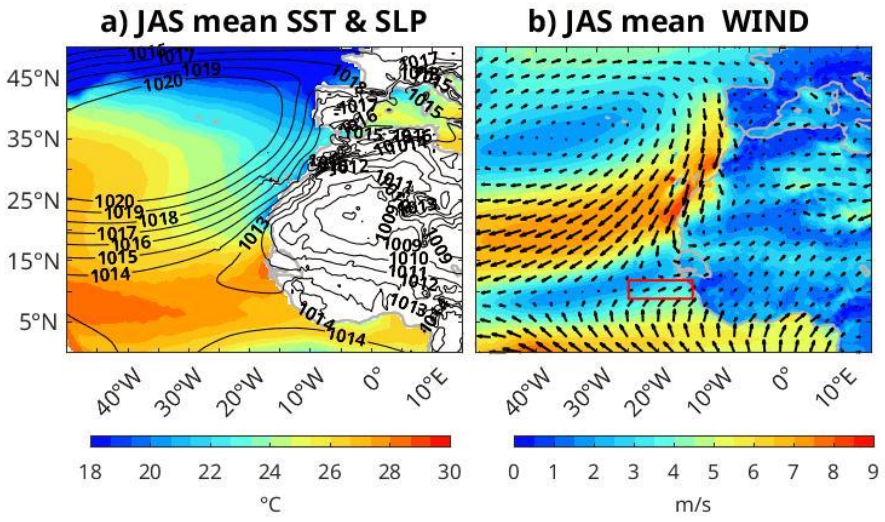

Figure 5. JAS 1979-2018 ERA5 reanalyses: a. SST (colors) and SLP (black contours). b. 10m-wind speed (colors) and direction (arrows). The red frame indicates the location of the WAWJ (25°W-14°W, 9°N-12°N).

Figure 6 presents the linear regression of SST, SLP and 10-meter wind on PC1CRU, with lags ranging from -2 (meaning the parameters precede PC1CRU by two months) to 0. Two months prior to a wet summer in Senegal, a significant negative SLP anomaly (exceeding -0.4 hPa) begins to emerge in the North Atlantic, reflecting a weakening of the Azores high (Figure 6, left, lag -2). This results in a weakening of the trade winds by approximately -0.3 m/s off Mauritania and Western Sahara (Figure 6, right), reducing the intensity of coastal upwelling and latent heat fluxes, thereby creating a warm SST anomaly off Senegal and Cap Blanc (Figure 6, left, lags -1). At lag -1, the subtropical SLP anomaly strengthens and extends over the continent to the eastern border of Mauritania (around 5°W) between 20°N and 30°N, with a significant weakening of the northeasterlies to -0.3 to -0.4 m/s off Senegal and Cap Blanc (between 10°N and 25°N). In response, the warm SST anomaly off Cap Blanc reaches +0.4°C at lag 0 and extends horizontally southwestward between 10°N and 15°N at 50°W. This small yet significant warming, owing to its extended coverage, could contribute to the formation of a negative pressure anomaly (exceeding -0.4 hPa) between 15°N and 25°N at lag 0 over the ocean (Figure 6, left, lag 0). This negative SLP anomaly indicates the northward shift of low-pressure systems within the marine ITCZ. The most significant anomalies it generates are primarily located in the southern half of the anomaly, between 10°N and 20°N. In this region, it decelerates surface winds in the north and intensifies them in the south (compare Figure 6, right, lag 0, and Figure 5b). Westerly anomalies are subsequently observed between 7°N and 12°N off the coast, signifying a strenghtening of the WAWJ. Finally, over the continent, a positive pressure signal is observed around 20°N to 30°N, associated with a less intense Heat Low than average. Although this signal is visible only at the 1000 hPa pressure level over the continent (not shown), its extension over the ocean is evident in the SLP anomaly near the coast around 25°N (Western Sahara).

A similar linear regression was conducted using the PC1CRU index calculated for the entire Sahel (not shown): no significant differences in surface wind or SLP were identified, which is expected given the strong correlation between the two indices. However, disparities in NETA SST anomalies, as discussed in the previous section, still exist: Senegal JAS precipitation, although sharing the majority of its interannual / summer monthly intraseasonal variance with the entire Sahel, appears to be influenced by a different SST anomaly: it supports the hypothesis that a regional feedback involving NETA SST, SLP and surface winds could be at work.

6 Moisture transport

The JAS average of the low-level moisture transport (integrated between 1000 hPa and 850 hPa) is plotted in Figure 7a. Over the ocean, it closely resembles the surface wind pattern (Figure 5b): moisture transport carried along by the trade winds, controlled by the Azores and Saint Helena anticyclones, converge between 8°N and 15°N. East of 30°W, at approximately 10°N, there is a notable inland-directed moisture transport, likely carried by the WAWJ, in agreement with Pu and Cook (2010, 2011), and Lélé et al. (2015).

The divergence of the moisture transport exhibits a zonal band of significant convergence along the ITCZ between 5°N and 13°N, slightly south of the wind maximum convergence (Figure 7c). This convergence aligns perfectly with the zonal band of average JAS precipitation (Figure 7e). The most significant precipitation is located along the coast (Figure 7c), induced by the strong coastal convergence of moisture transport driven by the WAWJ around 10°N and further south by the southern monsoon flux (Figure 7a). Indeed, given that the lower atmospheric layer is consistently close to moisture saturation in oceanic areas, near-surface convergence and precipitation are co-located most of the time (Weller et al., 2017).

Over the continent, there is a noticeable contrast in moisture transport patterns. To the south of 18°N, the moisture transport is south / southwestern and relatively in-

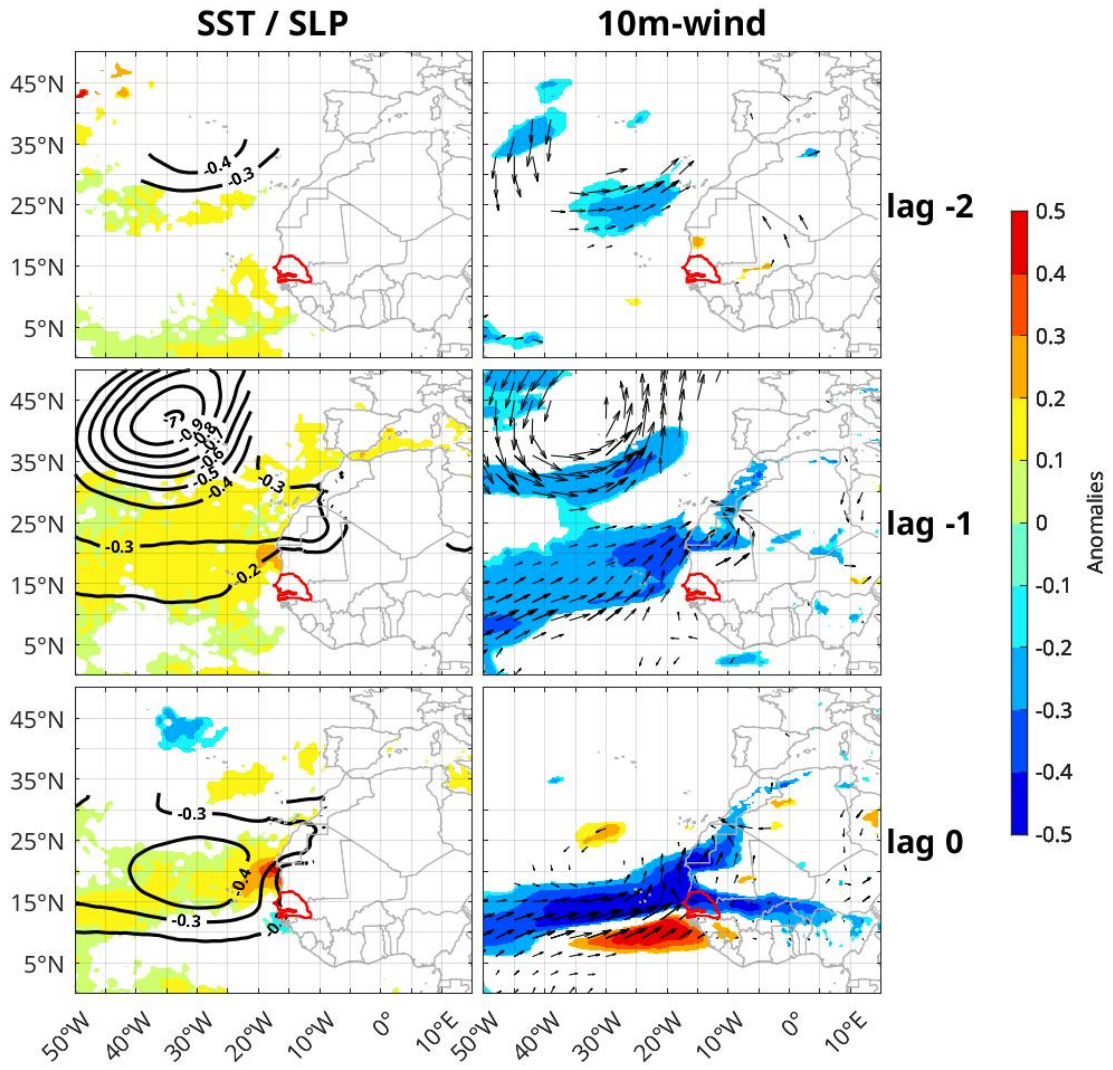

Figure 6. Linear regression of ERA5 reanalyses on PC1CRU, from lags -2 (ERA5 leads PC1CRU by 2 months) to lag 0. Left: SST (colors, °C) and SLP (black contours, hPa). Right: 10m-wind speed (colors, m/s) and direction (arrow). Only values significant at the 95% level are plotted.

tense. It strongly weakens north of 18°N and reaches a minimum in the core of the Heat Low (Figure 7a). This naturally leads to a notable convergence of moisture transport around 18°N, roughly corresponding to the "Intertropical Front", or "Intertropical Discontinuity" (ITD). However, unlike over the ocean, this pronounced near-surface convergence does not coincide with a precipitation peak: the latter is observed further south between 5°N and 15°N (Figure 7e). Indeed, precipitation is primarily associated with the formation of MCSs south of the AEJ, as mentioned in the introduction, and is more influenced by moisture transport convergence in the mid-to-high troposphere rather than in the lower troposphere.

A last notable feature of the mean moisture transport over the continent is a distinct weakening of the westerly flow around 10°N-10°W, where the largest mountain in Sierra Leone, the Loma Mansa, rises to almost 2000m in height (Figure 7a). More generally, the high relief near the coast contributes to the amplification of precipitation on the windward side of these mountains (Figure 7e), in agreement with Kante et al. (2020).

The linear regressions of low-level moisture transport, its divergence, and precipitation in JAS are presented in Figure 7 (right). Over the ocean, a wetter than usual summer in Senegal is associated with a cyclonic moisture transport anomaly that clearly corresponds to the negative SLP anomaly found previously between 10°N and 30°N (Figure 7b). The induced strengthening of the WAWJ in the southern edge of this anomaly results in an increase in eastward moisture transport between approximately 6°N and 12°N, while a decrease in westward transport is observed between 12°N and 16°N (Figure 7b). This leads to a significant increase in the coastal convergence of moisture transport between 6°N and 12°N (Figure 7d), and consequently, higher oceanic and coastal precipitation, with a maximum anomaly reaching up to 2 mm/day over the ocean between 8°N and 15°N (Figure 7f).

On the continent, there is a narrow zonal band of reduced moisture transport between 12°N and 15°N (Figure 7b), bordered by opposite positive anomalies further south and in the region of the Heat Low further north. Consequently, there is a zonal band of negative divergence anomaly to the south (around 10°N) and positive to the north (around 15°N) of this zonal band. The Heat Low anomaly probably explains most of the weak but highly correlated negative precipitation anomalies detected between 18°N and 25°N, as well as part of the positive precipitation anomalies between 10°N and 18°N (Figure 7f, black contours). The increase in Sahel precipitation is indeed mostly controlled by the weakening of the Heat Low in its southern half, which shifts moisture transport further north (Cook, 1999). However, the convergence anomalies (Figure 7d) may also contribute to the increase in precipitation between 10°N and 18°N, following the inland extension of the WAWJ acceleration and eastward moisture transport around 10°N.

These results highlight the complex nature of the atmospheric dynamics controlling precipitation in West Africa. They lend support to investigations of the ITCZ, moisture transport, and precipitation, spanning the entire troposphere. Two vertical meridional cross-sections are conducted on either side of the coast, one over the ocean, spanning from 22°W to 17°W, and the other to the east of Senegal, spanning from 10°W to 5°W. Note that the results presented below remain consistent when the width of the sections is slightly adjusted or increased by 5°. Horizontal divergence of moisture transport is calculated as in equation (4) (Figure 8, colors). Given that zonal transport (black contours) typically surpasses meridional transport above 850 hPa, only the former is plotted in the figures.

In the mean profile over the ocean, in the lower layer (below 850 hPa), we observe similar signals to those in Figure 7: framed by divergent moisture transports south of 5°N or north of 15°N, a robust convergence coincides with the peak of eastward moisture transport within the WAWJ between 5°N and 13°N (Figure 8a). It also coincides with the heaviest rainfall (Figure 8a, bottom panel, gray profile). This convergence results from the south and north trade winds meeting within the ITCZ, and an increase in eastward moisture transport toward the coast via the WAWJ around 10°N (Figure 8a, solid black contours). Above 850 hPa, there is an intense westward moisture transport between 750 and 550 hPa, at 12-18°N (Figure 8a, dashed black contours), indicating the presence of the AEJ. No signal is detected above 400 hPa, suggesting that moisture transport by the Tropical Easterly Jet, located at approximately 5°N between 100 and 200 hPa, is negligible.

In the mean profile over the continent, above 850 hPa, a similar maximum of zonal moisture transport is found at the location of the AEJ (Figure 8c, black contours). Be-

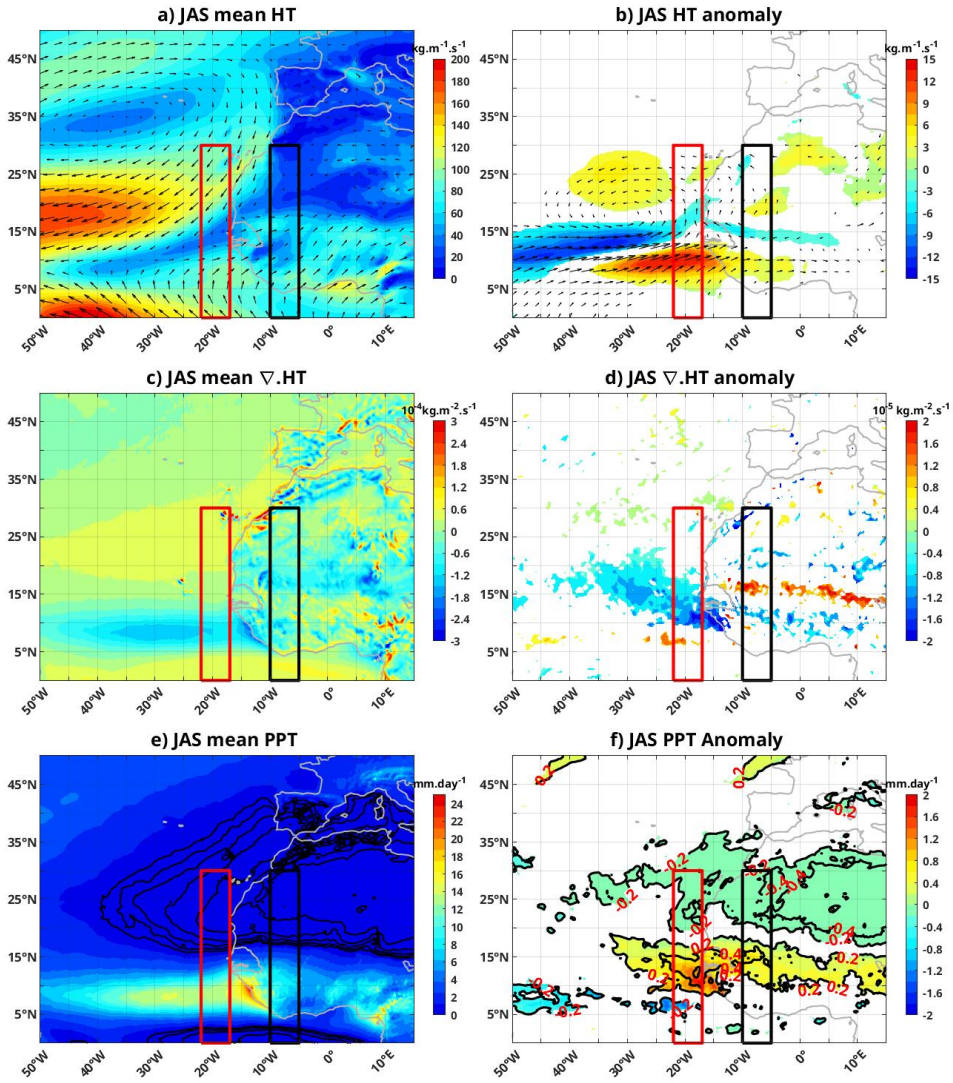

Figure 7. JAS 1978-2018 ERA5 reanalyses, average (left) and linear regression on PC1CRU index (right): a., b. magnitude (colors) and direction (arrow) of moisture transport (HT). c., d. divergence of moisture transport ($\nabla\cdot$ HT). e.,f. precipitation (PPT). In e., values less than 1 mm/day are outlined in black (intervals of 0.1 mm/d). In b., d. and f., only values significant at the 95% confidence level are plotted. In f., correlations are depicted using black contours with intervals of 0.2. Red and black frames indicate the location of the meridional-vertical sections plotted in Figures 8 and 9.

low 850 hPa, the western moisture transport extends as far north as 18°N (15°N over the ocean). A minimum in moisture transport convergence is found at 9-12°N, dividing the flow into two segments on either side of the Loma Mansa mountains as observed in Figure 7a. Strong convergence takes place at the bottom of the southern branch, explaining the heavy precipitation south of 10°N (Figure 8c, bottom panel). A second convergence maximum is observed in the northern branch, in the ITD region around 18°N, but it does not correspond to strong precipitation. The latter is governed by MCSs generated along the AEJ north of 17°N, as mentioned earlier, which probably explains why the precipitation peak is located around 10°N, at the latitude of the AEJ southern edge.

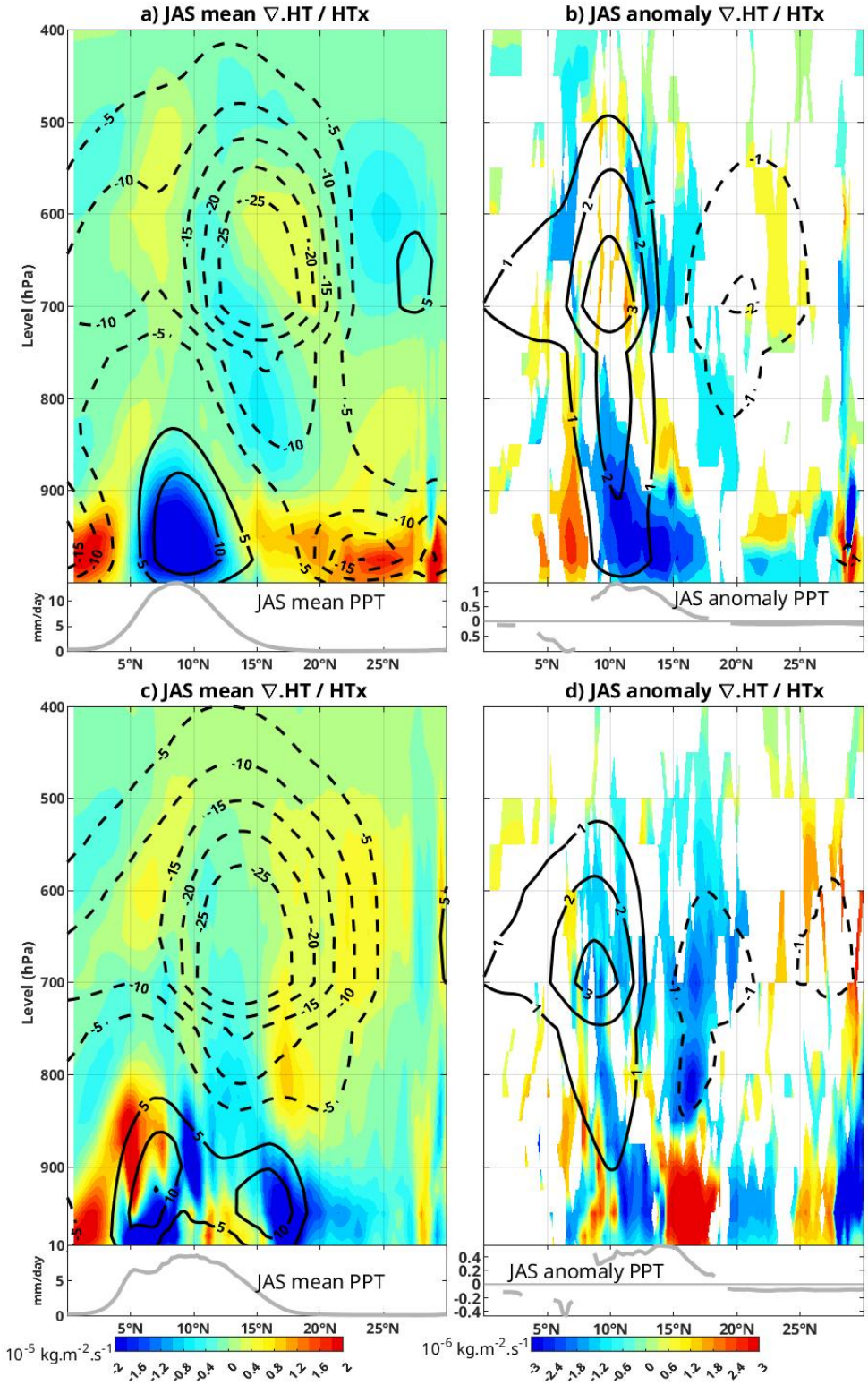

Figure 8. JAS 1978-2018 ERA5 reanalyses, average (left) and linear regressions on the PC1CRU index (right) in vertical meridional sections over the ocean (22°W-17°W, a., b.) and over the continent (10-5°W, c., d.): Divergence of moisture transport (colors) and zonal moisture transport (black contours, solid for positive, dashed for negative), superimposed on precipitation (gray line in panels at the bottom). Only values significant at the 95% confidence level are plotted.

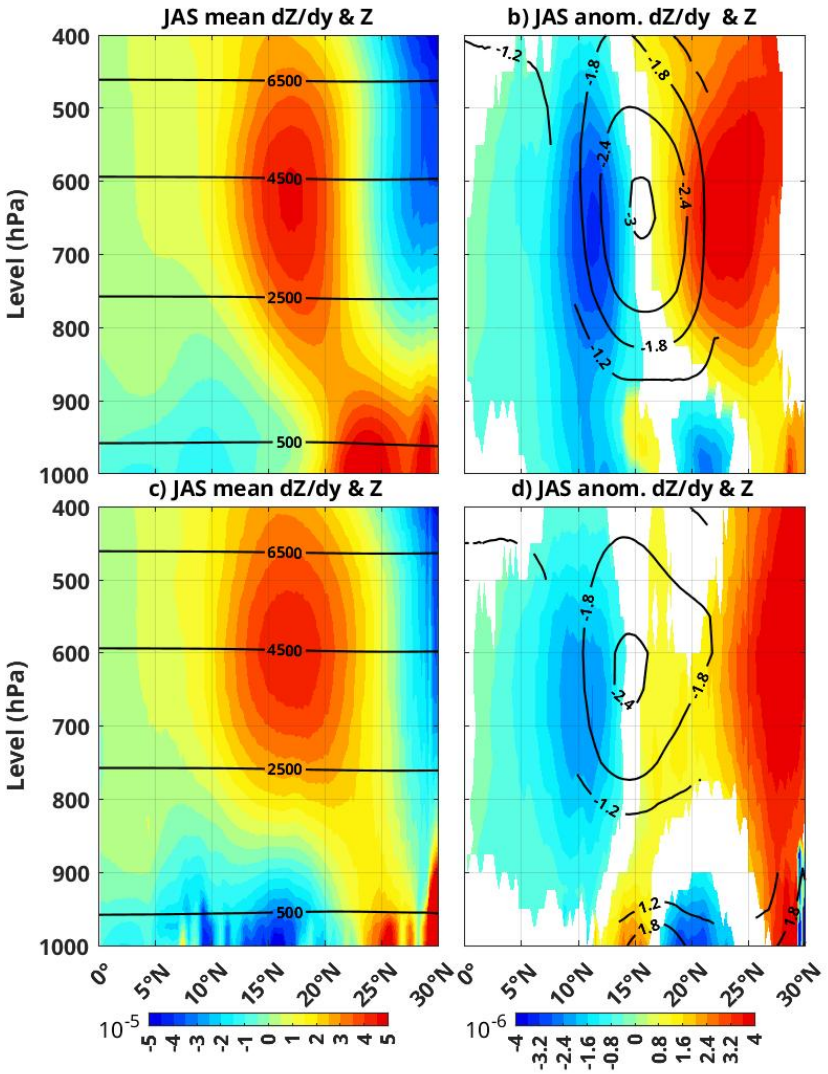

Figure 9. Same as Figure 8, but for geopotential height (black contours) and its meridional gradient (colors).

Over the ocean, the linear regression on PC1CRU shows an increase in low-level convergence of moisture transport between 9°N and 18°N (Figure 8b, colors), aligning with positive precipitation anomalies a few degrees north of their mean position (Figure 8b, bottom panel, grey profile). The increased convergence is caused by the acceleration of the WAWJ along its northern edge, as indicated by the positive anomaly in zonal transport between 9°N and 13°N (black contours). This anomaly extends in altitude up to about 500 hPa, peaking between 600 and 700 hPa: at this altitude, it indicates a deceleration of the AEJ on the southern edge of its mean position. At the same altitude, a negative anomaly in zonal transport is observed further north, around 20°N, indicating an acceleration of the AEJ on its northern edge: the AEJ has slightly shifted north.

In the linear regression over the continent, above 850 hPa, anomalies of zonal moisture transport resemble those over the ocean. However, the negative anomaly north of 15°N is less pronounced and extends further north (Figure 8d, black contours). More-

over, the positive anomaly between 9°N and 12°N remains above 850 hPa without reaching the surface, in contrast to the situation above the ocean. Below 850 hPa, alternating positive and negative divergence anomalies emerge approximately every 5°: north of 15°N, they probably result from the weakening of the Heat Low in its southern half, as mentioned earlier. However, between 10°N and 15°N, the convergence anomaly rather corresponds to a continental extension of the large WAWJ acceleration found over the ocean at the same latitude: it probably contributes significantly to the heavy precipitation observed between 10°N and 15°N.

In summary, the increase in summer precipitation in Senegal is partly of continental origin and controlled by the Heat Low and the AEJ. However, there are also clear signs of an influence coming from the Atlantic ocean through the WAWJ: a northward shift of the ITCZ comes with an intensification of the latter, which increases the western moisture transport between 10°N and 15°N and its convergence. It results in an increase in precipitation at the same latitudes. The SST could play a role in this intensification by altering low-level meridional pressure gradients through hydrostatic adjustment along its southern edge, along 10-15°N: the WAWJ would then respond to the pressure gradient signal via geostrophic adjustment. We test the plausibility of this hypothesis in the next section.

7 Geostrophic adjustment to the NETA SST anomaly

In this section, the geopotential height (or Z) at different pressure levels is used to calculate a meridional gradient (dZ/dy, colors): anomalies in dZ/dy can then be assimilated as anomalies in meridional pressure gradient of the same sign and provide information about the geostrophic zonal wind north of 5°N (geostrophic approximation is no longer valid near the equator), through the formula: $u_g = -\frac{g}{f}\frac{\partial Z}{\partial y}$.

A large peak of positive dZ/dy is found at 10-20°N around 500-700 hPa over the ocean (Figure 9a), emphasizing the clear geostrophic origin of the AEJ (Cook, 1999). Negative values of dZ/dy are found further north, indicating a high in the mid and upper tropospheric pressure around 20-25°N. Below 850 hPa, dZ/dy displays a negative value within the WAWJ (driving eastward geostrophic wind) south of 18°N and a positive value to the north (westward wind). The value of dZ/dy at 10°N is approximately -1 to -2 $\times 10^{-5}$ units, which corresponds to a geostrophic zonal wind speed of 3.8 to 7.8 m/s when multiplied by $-g/f$ (with $g = 9.81 m/s^2$, $f = 2\Omega \sin(10^o)$ and $\Omega = 2\pi$ rad / day), i.e. representative of the speeds typically found within the WAWJ. This is in line with Pu and Cook (2010) who show that while the jet is largely ageostrophic during its seasonal transitions, it is dominated by geostrophy on average.

The local negative minimum of dZ/dy around 10°N is located over an ocean region where the meridional SST gradient is positive and may reach a local maximum, as can be observed in Figure 5 (left). A positive maximum of dZ/dy is located further north around 23-25°N, over a strongly negative SST gradient in the southern front of the coastal upwelling off Cap Blanc. These alignments of dZ/dy and dSST/dy extrema are in agreement with the theory of Lindzen and Nigam (1987) suggesting that the near-surface pressure gradients adjust to the SST gradients. This is also in agreement with Diakhaté et al. (2018), who suggested that the equatorial low, thus the marine ITCZ, is partially controlled on its edges by meridional SST gradients.

A similar signature of the AEJ is found in the mid-troposphere above the continent, but the subtropical high is shifted north by 2 or 3 degrees (Figure 9c). Below 850 hPa, negative values of dZ/dy are found to the south and positive values to the north of the Heat Low, whose center is located around 20-25°N. Large values of dZ/dy at 25°N and at 16-17°N reflect the very steep "walls" of the Heat Low, with the southernmost corresponding to the ITD.

Above the continent, the linear regression of Z and dZ/dy on PC1CRU shows a significant drop in pressure within the AEJ, indicating its northward shift (weakening of easterlies in the southern half of its mean position, strengthening in the north, Figure 9d). The dominant signal in dZ/dy is a positive anomaly north of 15°N: as it is particularly intense north of 25°N, it likely reflects the influence of the large-scale subtropical atmospheric circulation and / or the Mediterranean. Extending down to the surface, this anomaly covers a positive pressure anomaly confined under 900 hPa between 15°N and 20°N, which reflects the weakening of the Heat Low in its southern half, inducing a northward shift of the pressure minimum. This is primarily what controls the northward shift of the MCSs path, thus partly explaining the increase in precipitation between 10°N and 18°N in Senegal. However, the signal corresponding to the weakening of the AEJ on its southern edge (negative anomalies in dZ/dy around 10°N at 600-700 hPa) appears to be somewhat weaker, and does not reach the surface, suggesting it is an eastward extension of a similar anomaly found above the ocean.

Above the ocean, the overall anomalies in dZ/dy are similar to those over the continent, with a slight northward shift of one or two degrees (Figure 9b). Below 850 hPa, the signals north of 15°N are likely an extension over the ocean of the anomalies observed above the continent, thus controlled by the variability of the Heat Low. However, south of 15°N, the negative anomaly of dZ/dy is significant between 8°N and 14°N, whereas it is not over the continent (Figure 9d). This suggests that it is forced by the SST anomaly. With a value of approximately -2×10^{-6} units, such a dZ/dy anomaly drives a geostrophic zonal wind anomaly of about 0.7 m/s, which is of the same magnitude than the surface wind anomaly observed at the same latitudes (Figure 6, right, lag 0).

This highlights that the strenghtening of westerlies around 10°N-15°N, which corresponds to an acceleration of the WAWJ on its northern side and leads to increased precipitation in Senegal, is clearly a geostrophic response to near-surface pressure fluctuations. Since the latter is likely controlled by the SST warm anomaly between 10°N and 20°N, via the mechanism theorized in Lindzen and Nigam (1987), this suggests the existence of a regional feedback mechanism between SST and surface winds in the NETA.

8 Discussion and conclusions

This work documents the oceanic and atmospheric signals related to monthly precipitation from July to September in Senegal, using CRU observations and ERA5 reanalyses covering the period from 1979 to 2018 (40 years). It compares the signals related to precipitation variability in Senegal versus the entire Sahel region. Noting a significant difference in Northeast Tropical Atlantic (NETA) SST, it takes a closer look at surface signals (pressure, wind, and moisture transport) and along two vertical sections in the mid and lower troposphere. Finally, it proposes a mechanism linking NETA SST to precipitation in Senegal.

First, monthly precipitation values in Senegal for 40 years are used. Anomalies for the months of July to September are extracted, and an EOF decomposition is performed: this yields an index, PC1CRU. This index characterizes interannual variability, but since three successive monthly values per year are retained, it also captures some intraseasonal variability in JAS. This mode is highly significant, as it explains two-thirds of the total precipitation variance in Senegal, with a pattern of anomalies of the same sign across the country and a strong gradient in their amplitude, from very weak in the north to very strong in the southwest of Senegal.

A comparison with a similar index calculated using ERA5 reanalysis precipitation data shows good correspondence, which suggests using the SST and atmospheric parameters from these reanalyses to explore the dynamic environment of the dominant mode, PC1CRU, in Senegal's precipitation variability. All subsequent analyses are therefore based

on linear regressions performed on this index. It should be noted that the results are presented for a positive anomaly of PC1CRU, indicating increased precipitation, but similar discussions would apply to a negative anomaly, as the regression is linear.

Increased JAS precipitation in Senegal is generally preceded by cold SST anomalies in the eastern equatorial Pacific (La Niña event) and warm SST anomalies in the Mediterranean Sea. These results are in line with many previous studies, including those by Rowell (2001), Giannini et al. (2003), Mohino et al. (2011), Rodríguez-Fonseca et al. (2011), and Diakhate et al. (2019). However, we obtained much weaker correlations than in these studies, especially in the East Equatorial Pacific and the Mediterranean, because we used a Senegal precipitation index instead of a Sahel one. Moreover, completely different anomalies are found in the NETA: this suggests that the western part of the Sahel, as Senegal, is more influenced by the Atlantic Ocean and less by large-scale atmospheric forcing and teleconnections than the entire Sahel. Therefore, the atmospheric dynamic anomalies in the NETA related to increased JAS precipitation in Senegal are examined.

The main result obtained indicates that increased JAS precipitation in Senegal is attributed to the increased convergence of low-level moisture transport, driven by an increase in the West African Westerly Jet (WAWJ). It also appears to be linked to the northward shift of the African Easterly Jet (AEJ) between 750 hPa and 550 hPa.

Above the continent, just east of Senegal, this northward shift of the AEJ is likely due to a northward migration of the Heat Low, in agreement with previous studies such as Diallo et al. (2013) and Sylla et al. (2013) that used regional climate models, or Grist and Nicholson (2001) and Dezfuli and Nicholson (2011) who used reanalysis data. Atmospheric teleconnections, both regional and larger scale with ENSO or Mediterranean SSTs, are also likely to play an important role. This probably leads to a northward migration of the trajectories of the Mesoscale Convective Systems (MCSs) responsible for most of the summer precipitation, explaining their increase between 10°N and 15°N.

However, over the ocean, just west of Senegal, the same northward shift of the AEJ as over the continent is observed, but the increase in precipitation is largely explained by an increase in low-level moisture transport convergence, created by an acceleration of the WAWJ. This is controlled by a significant negative pressure anomaly located in the NETA (10°N-30°N), reflecting the northward movement of the low-pressure areas characterizing the marine ITCZ. This negative pressure anomaly is situated above a positive SST anomaly, and the near-surface winds anomalies are compatible with a geostrophic response of the WAWJ to a reinforcement of the negative meridional pressure gradient between 10°N and 15°N.The latter could itself result from an increase in the positive SST gradient on the southern edge of the warm anomaly, following the mechanism proposed by Lindzen and Nigam (1987). The SST - surface wind feedback mechanism would then be as follows: first, the northeastern Trade Winds weaken, forcing a warming of the SST between 10°N and 25°N. Second, the SLP adjusts to the warmer SST and becomes weaker between 10°N and 25°N; its increased negative meridional gradient to the south forces a strengthening of the near-surface winds in the WAWJ region. This eventually results in an increased convergence of moisture transport and precipitation between 10°N and 15°N.

Between these two zones (ocean and continent), Senegal likely receives the influence of atmospheric teleconnections and the Mediterranean through the mode of variability it shares with the Sahel, but it could also be strongly influenced by NETA SST through the previously suggested feedback mechanism. As the initial Trade Winds anomaly seems driven by an anomaly of the Azores High, hence linked to the North Atlantic Oscillation (NAO), these results could possibly explain the link between Sahel precipitation and the North Atlantic, as shown for example in Paeth and Friederichs (2004). However, the ocean-atmosphere feedback mechanism suggested in this study needs further exploration at shorter time scales than the monthly data presented here, as the atmo-

spheric response to SST fluctuations is very rapid (within hours/days). Therefore, further studies using daily data or a regional atmospheric model are needed to confirm or refute this potential role of NETA SST feedback on the WAWJ. This could lead to a better understanding of the mechanisms driving precipitation variability in Senegal and, ultimately, to improved seasonal forecasts.

9 Open Research

Version 4.03 of CRU TS precipitation observation data covering the period from January 1901 to December 2018 (Harris et al., 2020) is available on `https://data.ceda.ac.uk/badc/cru/data/cru_ts/cru_ts_4.03/data7`

Monthly average ERA5 data on simple levels and pressure levels from 1940 to present are also available respectively at `https://cds.climate.copernicus.eu/doi/10.24381/cds.f17050d7` and at `https://cds.climate.copernicus.eu/doi/10.24381/cds.6860a573`.

Acknowledgments

This work was supported by the IRD (institut de Recherche pour le Développement throught PDI-MSC program (Programme Doctoral International- Modélisation des Systèmes Complexes). This work was also supported by the Laboratoire Mixte International ECLAIRS2.

Appendix A

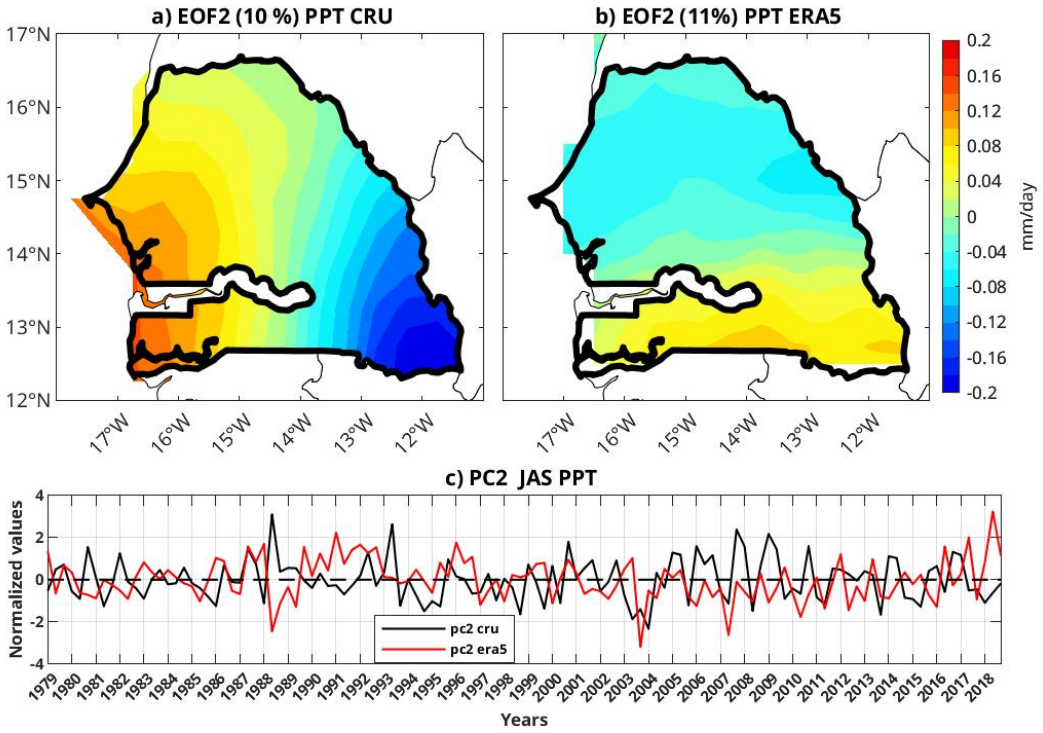

Figure A1. JAS 1979-2018 EOF2 of precipitation (mm/day): a. CRU observations, b. ERA5 reanalyses, and c. corresponding time series (black for CRU and red for ERA5).

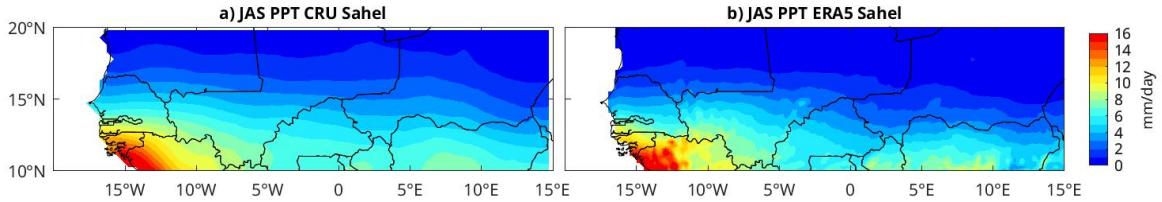

Figure A2. JAS 1978-2018 CRU (left) and ERA5 (right) precipitation.

	EOF1-Sn	EOF1-Sah	EOF2-Sn	EOF2-Sah
CRU	66.1%	41.6%	10%	9.3%
ERA5	48.5%	33%	11%	8.2%

Table A1. Percentage of total variance explained by EOF1 and EOF2 in Senegal and Sahel, using CRU or ERA5 precipitation.

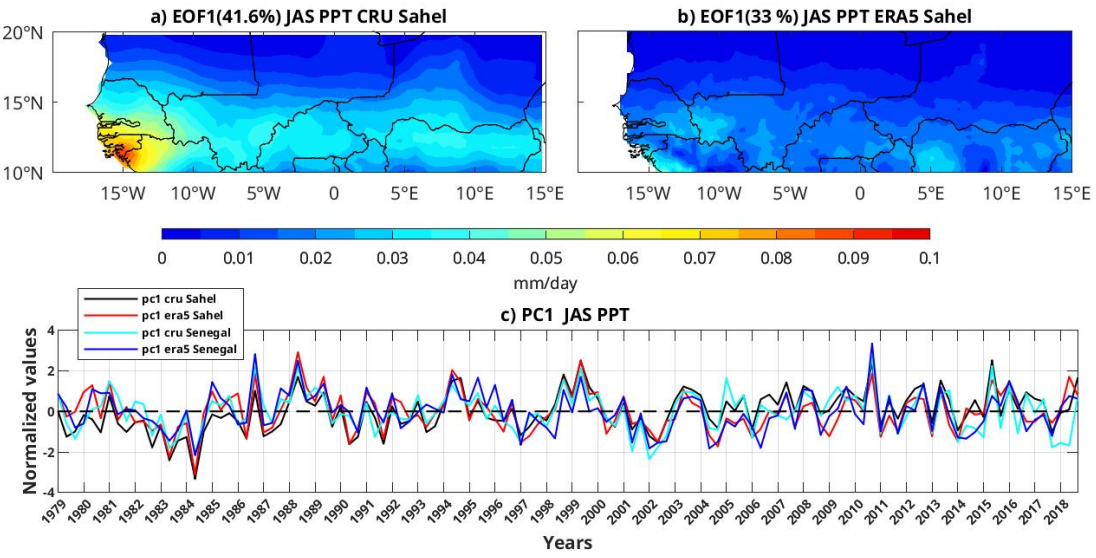

Figure A3. JAS 1979-2018 precipitation, EOF1 over the Sahel (mm/day): a. in CRU observations, b. in ERA5 reanalyses and c. their corresponding time series (CRU in black and ERA5 in red). CRU Senegal (cyan) and ERA5 Senegal (blue) time series are also plotted.

682

References

Bader, J., & Latif, M. (2003). The impact of decadal-scale indian ocean sea surface temperature anomalies on sahelian rainfall and the north atlantic oscillation. *Geophysical Research Letters*, *30*(22).

Biasutti, M., Held, I. M., Sobel, A. H., & Giannini, A. (2008). Sst forcings and sahel rainfall variability in simulations of the twentieth and twenty-first centuries. *Journal of Climate*, *21*(14), 3471–3486. doi: 10.1175/2007JCLI1896.1

Bonner, W. D. (1968). Climatology of the low level jet. *Monthly Weather Review*, *96*(12), 833–850. doi: 10.1175/1520-0493(1968)096⟨0833:COTLLJ⟩2.0.CO;2

Cabos, W., de la Vara, A., & Koseki, S. (2019). Tropical atlantic variability: Observations and modeling. *Atmosphere*, *10*(9). Retrieved from `https://www.mdpi.com/2073-4433/10/9/502`

Cadet, D. L., & Nnoli, N. O. (1987). Water vapour transport over africa and the atlantic ocean during summer 1979. *Quarterly Journal of the Royal Meteorological Society*, *113*(476), 581–602. doi: 10.1002/qj.49711347609

Camberlin, P., & Diop, M. (1999). Inter-relationships between groundnut yield in senegal, interannual rainfall variability and sea-surface temperatures. *Theoretical and Applied Climatology*, *63*(3), 163–181. doi: 10.1007/s007040050101

Camberlin, P., Janicot, S., & Poccard, I. (2001). Seasonality and atmospheric dynamics of the teleconnection between african rainfall and tropical sea-surface temperature: Atlantic vs. enso. *International Journal of Climatology*, *21*(8), 973–1005. doi: 10.1002/joc.673

Caminade, C., & Terray, L. (2010). Twentieth century sahel rainfall variability as simulated by the arpege agcm, and future changes. *Climate Dynamics*, *35*(1432-0894).

Caniaux, G., Giordani, H., Redelsperger, J.-L., Guichard, F., Key, E., & Wade, M. (2011). Coupling between the atlantic cold tongue and the west african monsoon in boreal spring and summer. *Journal of Geophysical Research: Oceans*, *116*(C4).

Cook, K. H. (1999). Generation of the african easterly jet and its role in determining west african precipitation. *Journal of Climate*, *12*(5), 1165 - 1184.

de Coëtlogon, G., Janicot, S., & Lazar, A. (2010). Intraseasonal variability of the ocean—atmosphere coupling in the gulf of guinea during boreal spring and summer. *Quarterly Journal of the Royal Meteorological Society*, *136*, 426–441. doi: 10.1002/qj.554

de Coëtlogon, G., Leduc-Leballeur, M., Meynadier, R., Bastin, S., Diakhaté, M., Eymard, L., ... Lazar, A. (2014). Atmospheric response to sea-surface temperature in the eastern equatorial atlantic at quasi-biweekly time-scales. *Quarterly Journal of the Royal Meteorological Society*, *140*(682). doi: 10.1002/qj.2250

Dezfuli, A. K., & Nicholson, S. E. (2011). A note on long-term variations of the african easterly jet. *International Journal of Climatology*, *31*(13), 2049–2054. doi: 10.1002/joc.2209

Diakhate, M., Rodriguez-Fonseca, B., Gomara, I., Mohino, E., Dieng, A. L., & Gaye, A. T. (2019). Oceanic forcing on interannual variability of sahel heavy and moderate daily rainfall. *Journal of Hydrometeorology*, *20*(3). doi: 10.1175/JHM-D-18-0035.1

Diakhaté, M., Lazar, A., de Coëtlogon, G., & Gaye, A. T. (2018). Do sst gradients drive the monthly climatological surface wind convergence over the tropical atlantic? *International Journal of Climatology*, *38*, e955–e965. doi: 10.1002/joc.5422

Diakhaté, M., Suárez-Moreno, R., Gómara, I., & Mohino, E. (2020). Statistical-observational analysis of skillful oceanic predictors of heavy daily precipitation events in the sahel. *Atmosphere*, *11*(6), 584. doi: 10.3390/atmos11060584

Diallo, I., Sylla, M. B., Camara, M., & Gaye, A. T. (2013). Interannual variability of rainfall over the sahel based on multiple regional climate models simulations.

Theoretical and Applied Climatology, *113*(1). doi: 10.1007/s00704-012-0791-y

Diatta, S., & Fink, A. H. (2014). Statistical relationship between remote climate indices and west african monsoon variability. *International Journal of Climatology*, *34*(12), 3348–3367. doi: 10.1002/joc.3912

Dommenget, D., & Latif, M. (2000). Interannual to decadal variability in the tropical atlantic. *Journal of Climate*, *13*(4), 777–792. doi: 10.1175/1520-0442(2000)013⟨0777:ITDVIT⟩2.0.CO;2

Fall, S., Semazzi, F. H. M., Dutta, D., Niyogi, S., Anyah, R. O., & Bowden, J. (2006). The spatiotemporal climate variability over senegal and its relationship to global climate. *International Journal of Climatology*, *26*(14), 2057–2076. doi: 10.1002/joc.1355

Folland, C., Palmer, T., & Parker, D. (1986). Sahel rainfall and worldwide sea temperatures, 1901-85. *Nature*, *320*(6063), 602–607. doi: 10.1038/320602a0

Foltz, G. R., & McPhaden, M. J. (2006). The role of oceanic heat advection in the evolution of tropical north and south atlantic sst anomalies. *Journal of Climate*, *19*(19), 6122–6138. doi: 10.1175/JCLI3961.1

Fontaine, B., Gaetani, M., Ullmann, A., & Roucou, P. (2011). Time evolution of observed july-september sea surface temperature-sahel climate teleconnection with removed quasi-global effect (1900-2008). *Journal of Geophysical Research-Atmospheres*, *116*, D04105. doi: 10.1029/2010JD014843

Fontaine, B., Garcia-Serrano, J., Roucou, P., Rodriguez-Fonseca, B., Losada, T., Chauvin, F., ... Janicot, S. (2009). Impacts of warm and cold situations in the mediterranean basins on the west african monsoon: observed connection patterns (1979–2006) and climate simulations. *Climate Dynamics*, *35*(1), 95–114. doi: 10.1007/s00382-009-0599-3

Fontaine, B., & Janicot, S. (1996). Sea surface temperature fields associated with west african rainfall anomaly types. *Journal of Climate*, *9*(11), 2935–2940. doi: 10.1175/1520-0442(1996)009⟨2935:SSTFAW⟩2.0.CO;2

Gaetani, M., Fontaine, B., Roucou, P., & Baldi, M. (2010). Influence of the mediterranean sea on the west african monsoon: Intraseasonal variability in numerical simulations. *Journal of Geophysical Research: Atmospheres*, *115*. doi: 10.1029/2010JD014436

Giannini, A., Saravanan, R., & Chang, P. (2003). Oceanic forcing of sahel rainfall on interannual to interdecadal time scales. *Science*, *302*(5647), 1027–1030. doi: 10.1126/science.1089357

Gomara, I., Mohino, E., Losada, T., Dominguez, M., Suarez-Moreno, R., & Rodriguez-Fonseca, B. (2017). Impact of dynamical regionalization on precipitation biases and teleconnections over west africa. *Climate Dynamics*, *50*(11), 4481–4506. doi: 10.1007/s00382-017-3886-4

Grace, K., & Davenport, F. (2021). Correction to: Climate variability and health in extremely vulnerable communities: investigating variations in surface water conditions and food security in the west african sahel. *Population and Environment*, *42*(4), 578–578. doi: 10.1007/s11111-021-00381-x

Grams, C. M., Jones, S. C., Marsham, J. H., Parker, D. J., Haywood, J. M., & Heuveline, V. (2010). The atlantic inflow to the saharan heat low: observations and modelling. *Quarterly Journal of the Royal Meteorological Society*, *136*, 125–140. doi: 10.1002/qj.429

Grist, J. P., & Nicholson, S. E. (2001). A study of the dynamic factors influencing the rainfall variability in the west african sahel. *Journal of Climate*, *14*(7), 1337–1359. doi: 10.1175/1520-0442(2001)014⟨1337:ASOTDF⟩2.0.CO;2

Grodsky, S. A. (2003). Near surface westerly wind jet in the atlantic itcz. *Geophysical Research Letters*, *30*(19), 2009. doi: 10.1029/2003GL017867

Gu, G. (2010). *Summer-time rainfall variability in the tropical atlantic* (S. W. Simard & M. E. Austin, Eds.). Intech Europe.

Gu, G., & Adler, R. F. (2009). Interannual variability of boreal summer rainfall in

the equatorial atlantic. *International Journal of Climatology*, *29*(2), 175–184. doi: 10.1002/joc.1724

Hagos, S. M., & Cook, K. H. (2008). Ocean warming and late-twentieth-century sahel drought and recovery. *Journal of Climate*, *21*(15), 3797–3814. doi: 10.1175/2008JCLI2055.1

Harris, I., Osborn, T. J., Jones, P., & Lister, D. (2020). Version 4 of the cru ts monthly high-resolution gridded multivariate climate dataset. *Scientific Data*, *7*(1), 109. doi: 10.1038/s41597-020-0453-3

Janicot, S., Harzallah, A., Fontaine, B., & Moron, V. (1998). West african monsoon dynamics and eastern equatorial atlantic and pacific sst anomalies (1970-88). *Journal of Climate*, *11*(8), 1874–1882. doi: 10.1175/1520-0442-11.8.1874

Janicot, S., Trzaska, S., & Poccard, I. (2001). Summer sahel-enso teleconnection and decadal time scale sst variations. *Climate Dynamics*, *18*(3), 303–320. doi: 10.1007/s003820100172

Joly, M., & Voldoire, A. (2009). Influence of enso on the west african monsoon: Temporal aspects and atmospheric processes. *Journal of Climate*, *22*(12), 3193–3210. doi: 10.1175/2008JCLI2450.1

Jung, T., Ferranti, L., & Tompkins, A. M. (2006). Response to the summer of 2003 mediterranean sst anomalies over europe and africa. *Journal of Climate*, *19*(20), 5439–5454. doi: 10.1175/JCLI3916.1

Kante, I. K., Sall, S. M., Badiane, D., Diouf, I., Dieng, A. L., Diaby, I., & Guichard, F. (2020). Analysis of rainfall dynamics in conakry, republic of guinea. *Atmospheric and Climate Sciences*, *10*(1), 1. doi: 10.4236/acs.2020.101001

Lavaysse, C., Flamant, C., Janicot, S., Parker, D. J., Lafore, J.-P., Sultan, B., & Pelon, J. (2009). Seasonal evolution of the west african heat low: a climatological perspective. *Climate Dynamics*, *33*(2), 313–330. doi: 10.1007/s00382-009-0553-4

Le Barbé, L., & Lebel, T. (1997). Rainfall climatology of the hapex-sahel region during the years 1950–1990. *Journal of hydrology*, *188*, 43–73.

Lebel, T., Diedhiou, A., & Laurent, H. (2003). Seasonal cycle and interannual variability of the sahelian rainfall at hydrological scales. *Journal of Geophysical Research: Atmospheres*, *108*. doi: 10.1029/2001JD001580

Lindzen, R. S., & Nigam, S. (1987). On the role of sea surface temperature gradients in forcing low-level winds and convergence in the tropics. *Journal of the Atmospheric Sciences*, *44*(17), 2418–2436. doi: 10.1175/1520-0469(1987)044⟨2418:OTROSS⟩2.0.CO;2

Liu, W., Cook, K. H., & Vizy, E. K. (2020). Role of the west african westerly jet in the seasonal and diurnal cycles of precipitation over west africa. *Climate Dynamics*, *54*(1), 843–861. doi: 10.1007/s00382-019-05035-1

Liu, Y., Chiang, J. C. H., Chou, C., & Patricola, C. M. (2014). Atmospheric teleconnection mechanisms of extratropical north atlantic sst influence on sahel rainfall. *Climate Dynamics*, *43*, 2797 - 2811.

Losada, T., Rodríguez-Fonseca, B., Polo, I., Janicot, S., Gervois, S., Chauvin, F., & Ruti, P. (2010). Tropical response to the atlantic equatorial mode: Agcm multimodel approach. *Climate Dynamics*, *35*(1), 45–52. doi: 10.1007/s00382-009-0624-6

Lélé, M. I., Leslie, L. M., & Lamb, P. J. (2015). Analysis of low-level atmospheric moisture transport associated with the west african monsoon. *Journal of Climate*, *28*(11), 4414–4430. doi: 10.1175/JCLI-D-14-00746.1

Meynadier, R., de Coëtlogon, G., Leduc-Leballeur, M., Eymard, L., & Janicot, S. (2016). Seasonal influence of the sea surface temperature on the low atmospheric circulation and precipitation in the eastern equatorial atlantic. *Climate Dynamics*, *47*(1432-0894).

Mo, K., Bell, G. D., & Thiaw, W. M. (2001). Impact of sea surface temperature anomalies on the atlantic tropical storm activity and west african

rainfall. *Journal of the Atmospheric Sciences*, *58*(22), 3477–3496. doi: 10.1175/1520-0469(2001)058⟨3477:IOSSTA⟩2.0.CO;2

Mohino, E., Rodríguez-Fonseca, B., Mechoso, C. R., Gervois, S., Ruti, P., & Chauvin, F. (2011). Impacts of the tropical pacific/indian oceans on the seasonal cycle of the west african monsoon. *Journal of Climate*, *24*(15), 3878–3891. doi: 10.1175/2011JCLI3988.1

Monerie, P.-A., Sanchez-Gomez, E., Gaetani, M., Mohino, E., & Dong, B. (2020). Future evolution of the sahel precipitation zonal contrast in cesm1. *Climate Dynamics*, *55*, 2801-2821.

Moron, V., Robertson, A. W., & Ward, M. N. (2006). Seasonal predictability and spatial coherence of rainfall characteristics in the tropical setting of senegal. *Monthly Weather Review*, *134*(11), 3248–3262. doi: 10.1175/MWR3252.1

Moron, V., & Ward, M. N. (1998). Enso teleconnections with climate variability in the european and african sectors. *Weather*, *53*(9), 287–295. doi: 10.1002/j.1477-8696.1998.tb06403.x

Nicholson, S. E. (2013). The west african sahel: A review of recent studies on the rainfall regime and its interannual variability. *International Scholarly Research Notices*, *2013*.

Nicholson, S. E., & Palao, I. (1993). A reevaluation of rainfall variability in the sahel .1. characteristics of rainfall fluctuations. *International Journal of Climatology*, *13*(4), 371–389. doi: 10.1002/joc.3370130403

Paeth, H., & Friederichs, P. (2004). Seasonality and time scales in the relationship between global sst and african rainfall. *Climate Dynamics*, *23*(7), 815–837. doi: 10.1007/s00382-004-0466-1

Park, J.-Y., Bader, J., & Matei, D. (2015). Northern-hemispheric differential warming is the key to understanding the discrepancies in the projected sahel rainfall. *Nature Communications*, *6*. doi: 10.1038/ncomms6985

Parker, D., & Diop-Kane, M. (2017). *Meteorology of tropical west africa: The forecasters' handbook*. John Wiley & Sons, Ltd.

Polo, I., Rodriguez-Fonseca, B., Losada, T., & Garcia-Serrano, J. (2008). Tropical atlantic variability modes (1979-2002). part i: Time-evolving sst modes related to west african rainfall. *Journal of Climate*, *21*(24), 6457–6475. doi: 10.1175/2008JCLI2607.1

Pu, B., & Cook, K. H. (2010). Dynamics of the west african westerly jet. *Journal of Climate*, *23*(23), 6263–6276. doi: 10.1175/2010JCLI3648.1

Pu, B., & Cook, K. H. (2011). Role of the west african westerly jet in sahel rainfall variations. *Journal of Climate*, *25*(8), 2880–2896. doi: 10.1175/JCLI-D-11-00394.1

Pu, B., & Cook, K. H. (2012). Role of the west african westerly jet in sahel rainfall variations. *Journal of Climate*, *25*(8), 2880–2896. doi: 10.1175/JCLI-D-11-00394.1

Quagraine, K. A., Nkrumah, F., Klein, C., Klutse, N. A. B., & Quagraine, K. T. (2020). West african summer monsoon precipitation variability as represented by reanalysis datasets. *Climate*, *8*(10), 111. doi: 10.3390/cli8100111

Rodríguez-Fonseca, B., Janicot, S., Mohino, E., Losada, T., Bader, J., Caminade, C., ... Voldoire, A. (2011). Interannual and decadal sst-forced responses of the west african monsoon. *Atmospheric Science Letters*, *12*(1), 67–74. doi: 10.1002/asl.308

Rowell, D. P. (2001). Teleconnections between the tropical pacific and the sahel. *Quarterly Journal of the Royal Meteorological Society*, *127*(575), 1683–1706. doi: 10.1002/qj.49712757512

Rowell, D. P. (2003). The impact of mediterranean ssts on the sahelian rainfall season. *Journal of Climate*, *16*(5), 849–862. doi: 10.1175/1520-0442(2003)016⟨0849:TIOMSO⟩2.0.CO;2

Rowell, D. P., Folland, C., Maskell, K., & Ward, M. (1995). Variability of summer

rainfall over tropical north-africa (1906-92) - observations and modeling. *Quarterly Journal of the Royal Meteorological Society*, *121*(523), 669–704. doi: 10.1002/qj.49712152311

Rust, H. W., Vrac, M., Sultan, B., & Lengaigne, M. (2013). Mapping weather-type influence on senegal precipitation based on a spatial–temporal statistical model. *Journal of Climate*, *26*(20), 8189–8209. doi: 10.1175/JCLI-D-12-00302.1

Semazzi, F., Mehta, V., & Sud, Y. (1988). An investigation of the relationship between sub-saharan rainfall and global sea surface temperatures. *Atmosphere-Ocean*, *26*(1), 118–138. doi: 10.1080/07055900.1988.9649293

Steinig, S., Harlass, J., Park, W., & Latif, M. (2018). Sahel rainfall strength and onset improvements due to more realistic atlantic cold tongue development in a climate model. *Scientific Reports*, *8*(2569).

Stensrud, D. J. (1996). Importance of low-level jets to climate: A review. *Journal of Climate*, *9*(8), 1698–1711. doi: 10.1175/1520-0442(1996)009⟨1698:IOLLJT⟩2.0.CO;2

Sultan, B., & Janicot, S. (2000). Abrupt shift of the itcz over west africa and intra-seasonal variability. *Geophysical Research Letters*, *27*(20), 3353–3356. doi: 10.1029/1999GL011285

Sultan, B., Labadi, K., Guégan, J.-F., & Janicot, S. (2005). Climate drives the meningitis epidemics onset in west africa. *PLOS Medicine*, *2*(1), e6. doi: 10.1371/journal.pmed.0020006

Suárez-Moreno, R., Rodríguez-Fonseca, B., Barroso, J. , & Fink, A. (2018). Interdecadal changes in the leading ocean forcing of sahelian rainfall interannual variability: Atmospheric dynamics and role of multidecadal sst background. *Journal of Climate*. doi: 10.1175/JCLI-D-17-0367.1

Sylla, M. B., Giorgi, F., Coppola, E., & Mariotti, L. (2013). Uncertainties in daily rainfall over africa: assessment of gridded observation products and evaluation of a regional climate model simulation. *International Journal of Climatology*, *33*(7), 1805–1817. doi: 10.1002/joc.3551

Thorncroft, C. D., Nguyen, H., Zhang, C., & Peyrillé, P. (2011). Annual cycle of the west african monsoon: regional circulations and associated water vapour transport: Annual cycle of west african monsoon. *Quarterly Journal of the Royal Meteorological Society*, *137*(654), 129–147. doi: 10.1002/qj.728

Vizy, E. K., & Cook, K. H. (2001). Mechanisms by which gulf of guinea and eastern north atlantic sea surface temperature anomalies can influence african rainfall. *Journal of Climate*, *14*(5), 795–821. doi: 10.1175/1520-0442(2001)014⟨0795:MBWGOG⟩2.0.CO;2

Von Storch, H., & Zwiers, F. W. (1999). *Statistical analysis in climate research*. Cambridge University Press. doi: 10.1017/CBO9780511612336

Wade, M., Mignot, J., Lazar, A., Gaye, A. T., & Carre, M. (2015). On the spatial coherence of rainfall over the saloum delta (senegal) from seasonal to decadal time scales. *Frontiers in Earth Science*, *3*. doi: 10.3389/feart.2015.00030

Wang, C. (2019). Three-ocean interactions and climate variability: a review and perspective. *Climate Dynamics*, *53*, 5119-5136.

Wang, C., Dong, S., Evan, A. T., Foltz, G. R., & Lee, S.-K. (2012). Multidecadal covariability of north atlantic sea surface temperature, african dust, sahel rainfall, and atlantic hurricanes. *Journal of Climate*, *25*(15), 5404 - 5415.

Ward, M. N. (1998). Diagnosis and short-lead time prediction of summer rainfall in tropical north africa at interannual and multidecadal timescales. *Journal of Climate*, *11*(12), 3167–3191. doi: 10.1175/1520-0442(1998)011⟨3167:DASLTP⟩2.0.CO;2

Weller, E., Shelton, K., Reeder, M. J., & Jakob, C. (2017). Precipitation associated with convergence lines. *Journal of Climate*, *30*(9), 3169 - 3183.

Worou, K., Goosse, H., Fichefet, T., Guichard, F., & Diakhate, M. (2020). In-

terannual variability of rainfall in the guinean coast region and its links with sea surface temperature changes over the twentieth century for the different seasons. *Climate Dynamics*, *55*(3), 449–470. doi: 10.1007/s00382-020-05276-5

Xie, S.-P., & Carton, J. (2004). Tropical atlantic variability: Patterns, mechanisms, and impacts. *Earth Clim*, *147*. doi: 10.1029/147GM07

Yang, C., Leonelli, F. E., Marullo, S., Artale, V., Beggs, H., Nardelli, B. B., ... Pisano, A. (2021). Sea surface temperature intercomparison in the framework of the copernicus climate change service (c3s). *Journal of Climate*, *34*(13), 5257–5283. doi: 10.1175/JCLI-D-20-0793.1

Zebiak, S. (1993, 08). Air–sea interaction in the equatorial atlantic region. *Journal of Climate*, *6*, 1567-1586. doi: 10.1175/1520-0442(1993)006⟨1567:AIITEA⟩2.0.CO;2

Zeng, N., Neelin, J. D., Lau, K.-M., & Tucker, C. J. (1999). Enhancement of interdecadal climate variability in the sahel by vegetation interaction. *Science*, *286*(5444), 1537-1540. Retrieved from `https://www.science.org/doi/abs/10.1126/science.286.5444.1537` doi: 10.1126/science.286.5444.1537

Figure 1.

a) PPT CRU

b) PPT ERA5

mm/day
14
12.6
11.2
9.8
8.4
7
5.6
4.2
2.8
1.4
0

c) standard deviation PPT CRU

d) standard deviation PPT ERA5

mm/day
3
2.7
2.4
2.1
1.8
1.5
1.2
0.9
0.6
0.3
0

e) bias (ERA5-CRU)

f) standard deviation bias

17°N
16°N
15°N
14°N
13°N
12°N

17°W
16°W
15°W
14°W
13°W
12°W

mm/day
-3
-2.4
-1.8
-1.2
-0.6
0
0.6
1.2
1.8
2.4
3

Figure 2.

a) EOF1 (66.1%) PPT CRU

b) EOF1 (48.5%) PPT ERA5

17°N
16°N
15°N
14°N
13°N
12°N

17°W
16°W
15°W
14°W
13°W
12°W

0.2
0.18
0.16
0.14
0.12
0.1
0.08
0.06
0.04
0.02
0
mm/day

c) PC1 JAS PPT

pc1 cru
pc1 era5

Normalized values

4
2
0
-2
-4

1979 1980 1981 1982 1983 1984 1985 1986 1987 1988 1989 1990 1991 1992 1993 1994 1995 1996 1997 1998 1999 2000 2001 2002 2003 2004 2005 2006 2007 2008 2009 2010 2011 2012 2013 2014 2015 2016 2017 2018

Years

Figure 3.

lag -5

lag -4

lag -3

lag -2

lag -1

lag 0

45°N
30°N
15°N
0°
15°S

180°W 140°W 100°W 60°W 20°W 20°E 60°E 100°E 140°E 180°E

SST anomalies (°C)

0.4
0.32
0.24
0.16
0.08
0
-0.08
-0.16
-0.24
-0.32
-0.4

Figure 4.

lag -5

lag -4

lag -3

lag -2

lag -1

lag 0

45°N
30°N
15°N
0°
15°S

180°W 140°W 100°W 60°W 20°W 20°E 60°E 100°E 140°E 180°E

SST anomalies (°C)

0.4
0.32
0.24
0.16
0.08
0
-0.08
-0.16
-0.24
-0.32
-0.4

Figure 5.

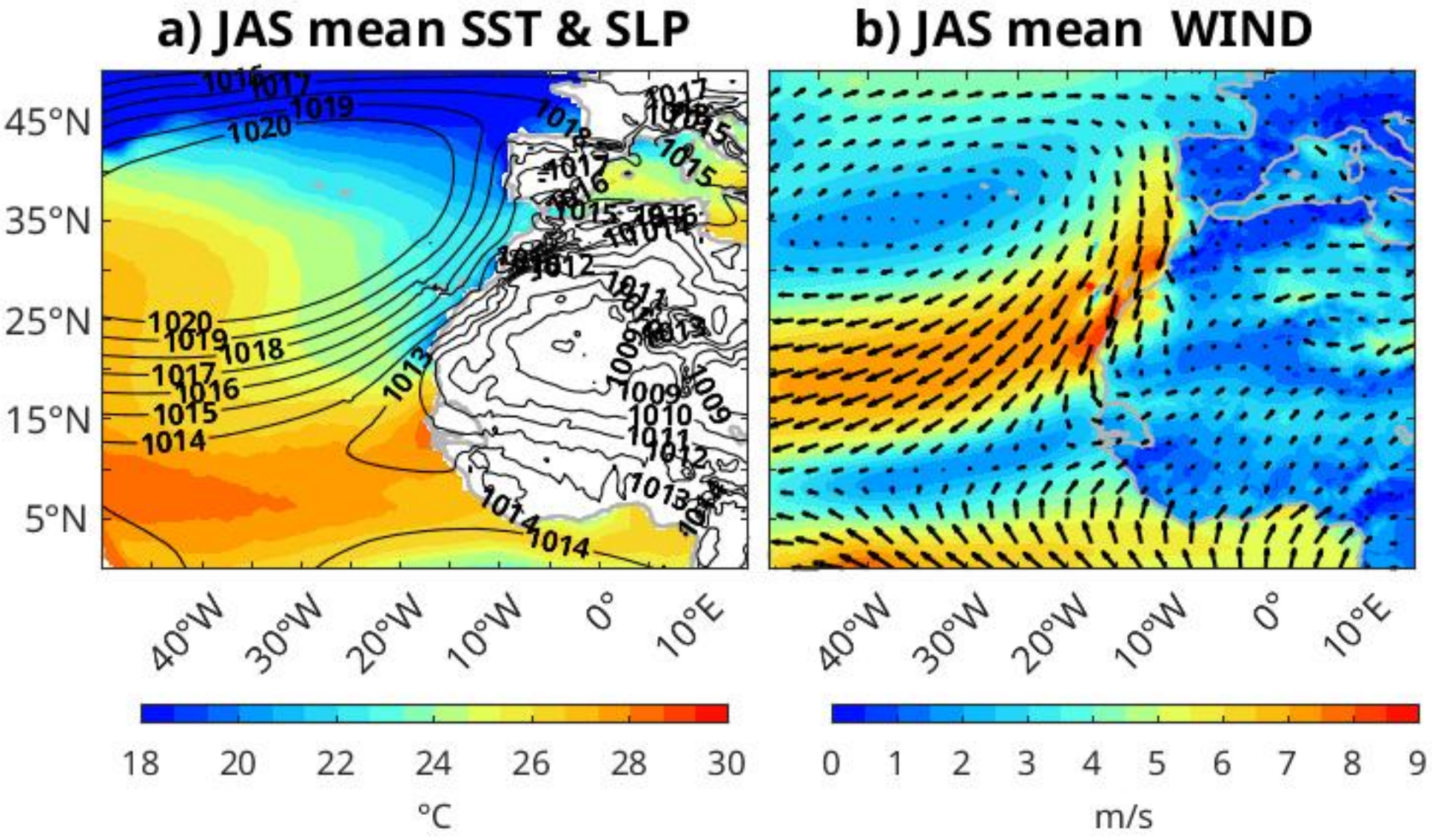
a) JAS mean SST & SLP
b) JAS mean WIND
45°N
35°N
25°N
15°N
5°N
40°W
30°W
20°W
10°W
0°
10°E
1020
1019
1018
1017
1016
1015
1014
1013
1012
1011
1010
1009
18
20
22
24
26
28
30
°C
0
1
2
3
4
5
6
7
8
9
m/s

Figure 6.

SST / SLP

10m-wind

lag -2

lag -1

lag 0

45°N
35°N
25°N
15°N
5°N

50°W
40°W
30°W
20°W
10°W
0°
10°E

-0.4
-0.3
-0.2
-0.1
-0.5
-0.6
-0.7
-0.8
-0.9
-1
0

0.5
0.4
0.3
0.2
0.1
0
-0.1
-0.2
-0.3
-0.4
-0.5

Anomalies

Figure 7.

a) JAS mean HT

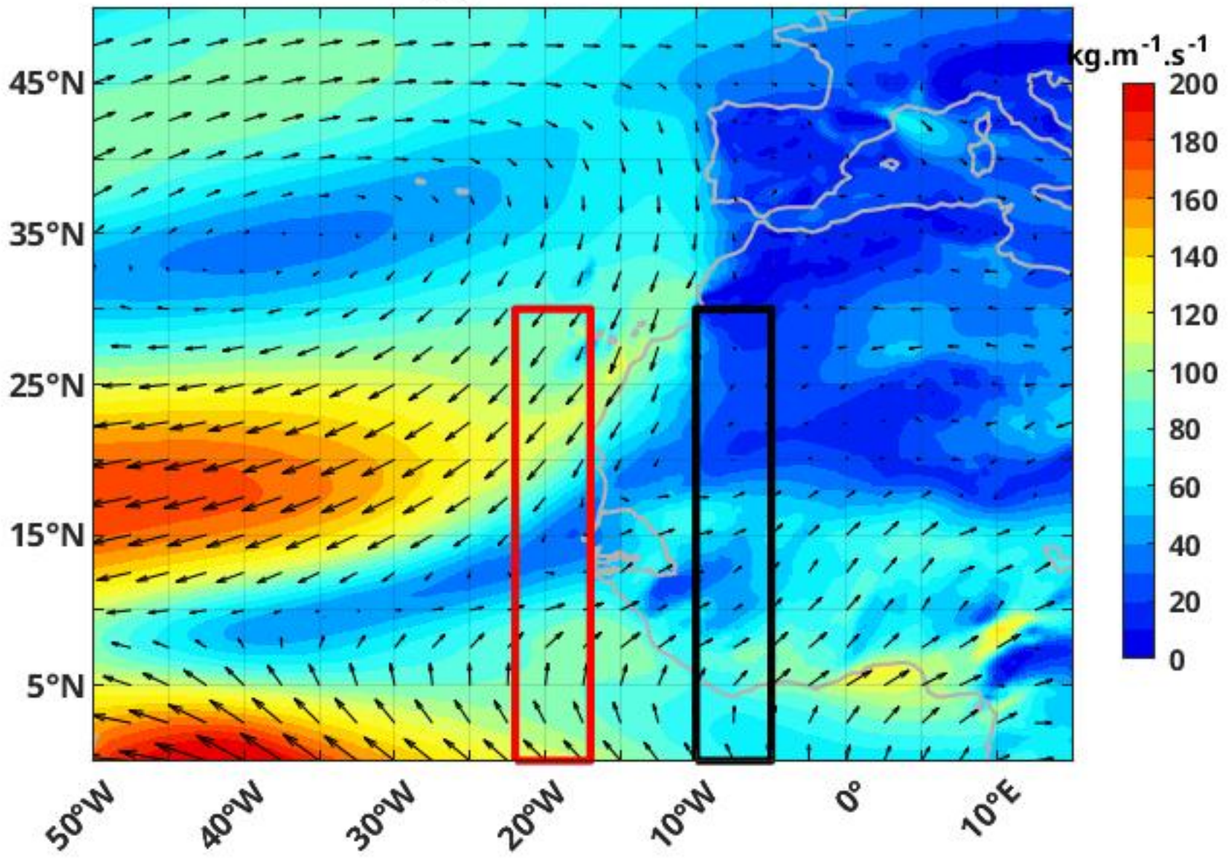

b) JAS HT anomaly

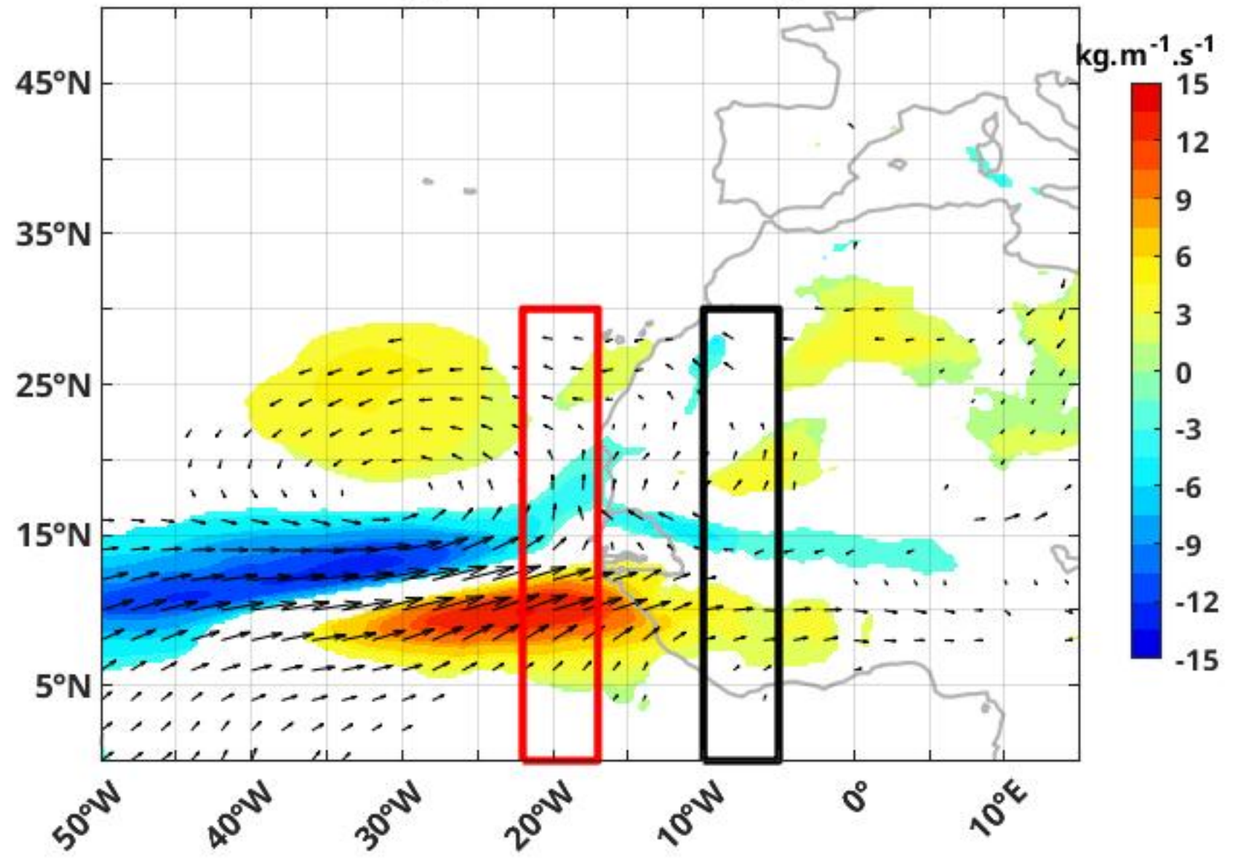

c) JAS mean ∇.HT

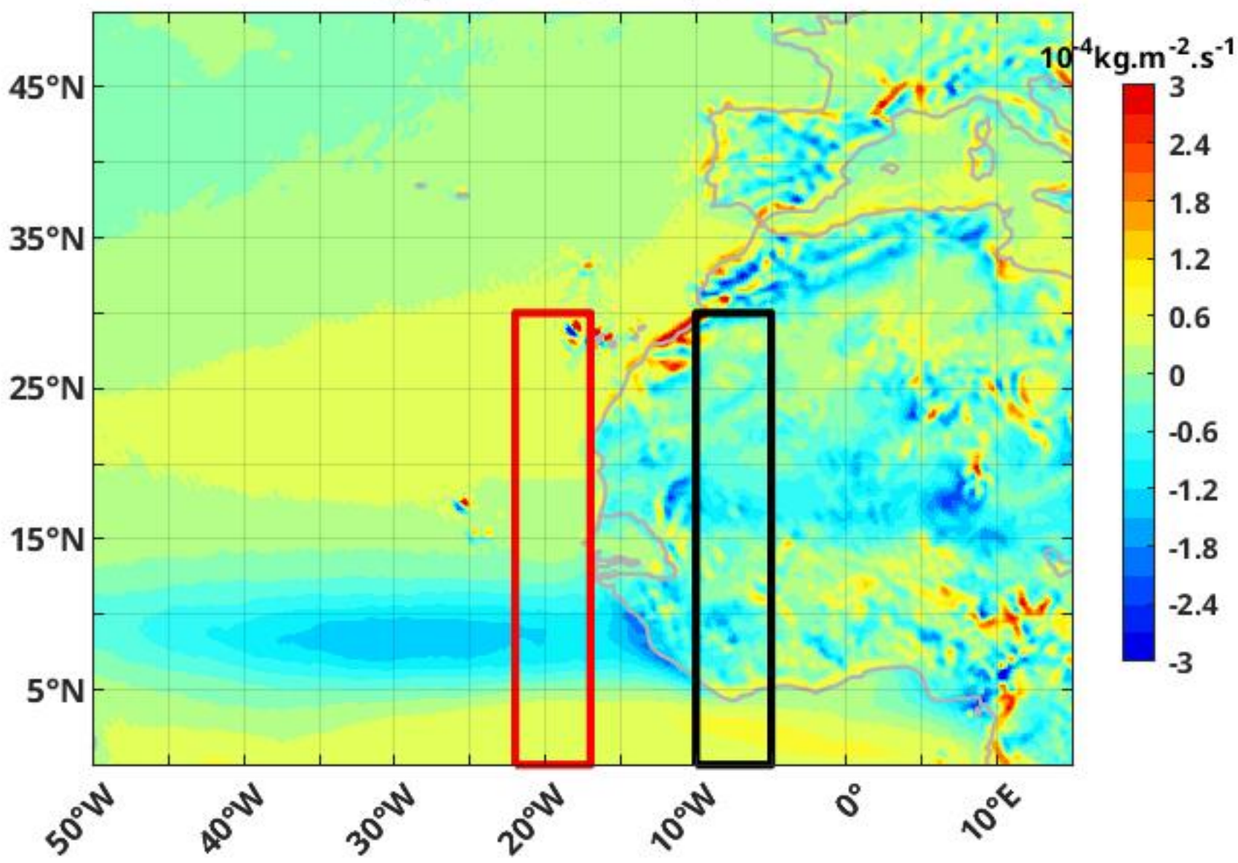

d) JAS ∇.HT anomaly

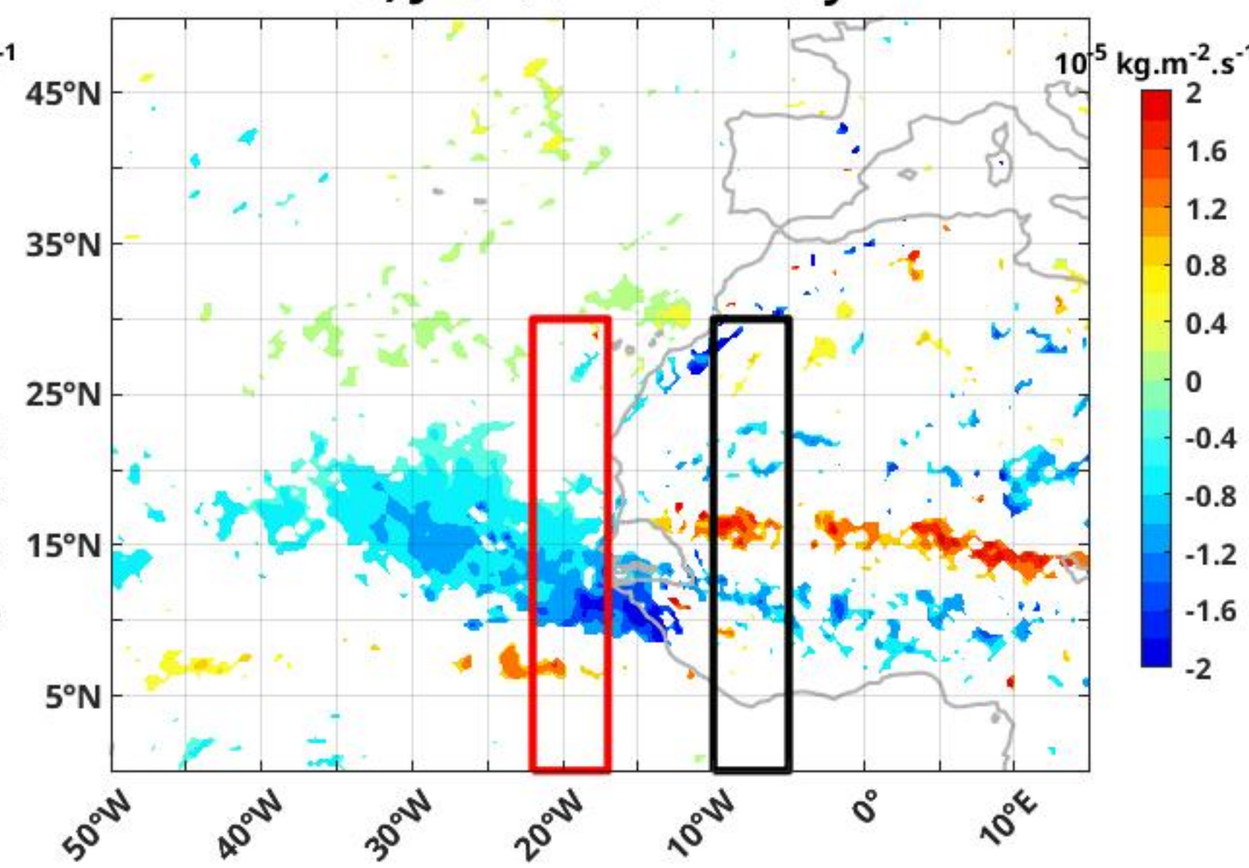

e) JAS mean PPT

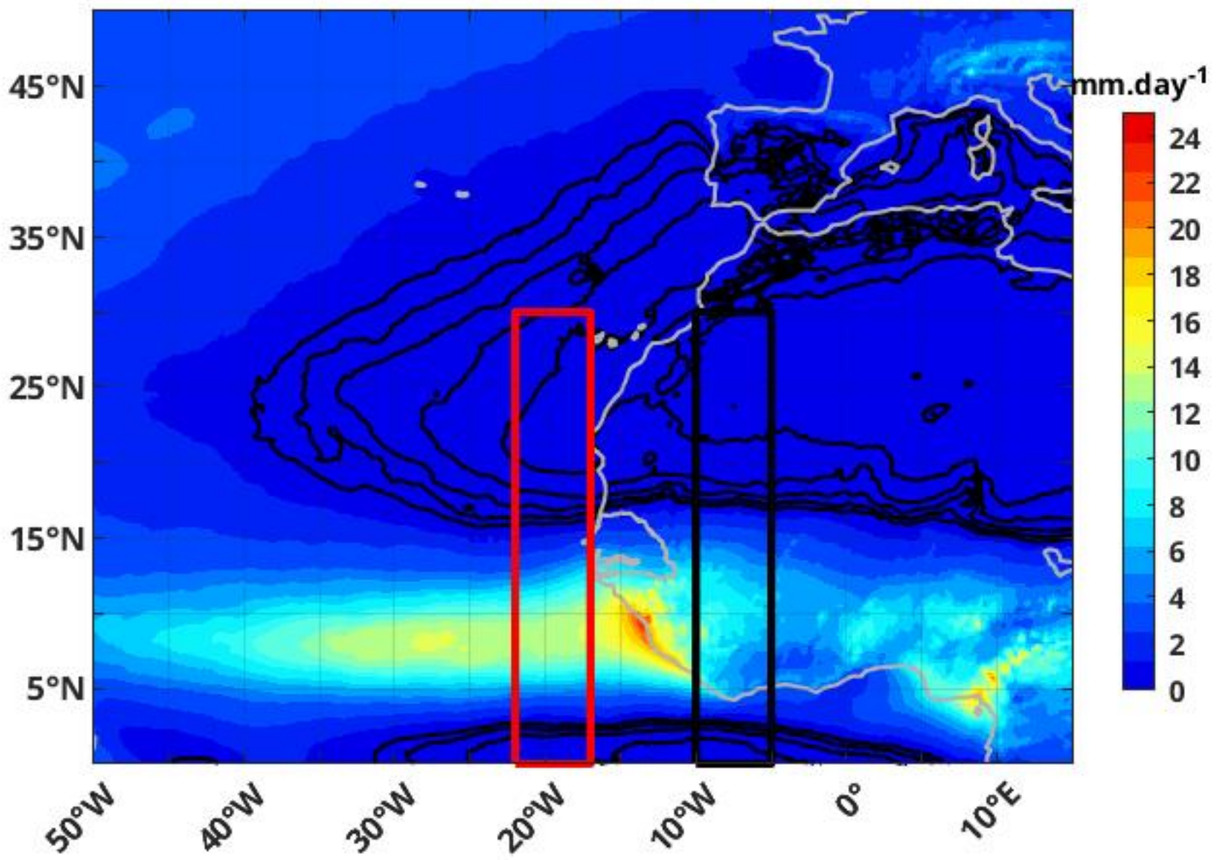

f) JAS PPT Anomaly

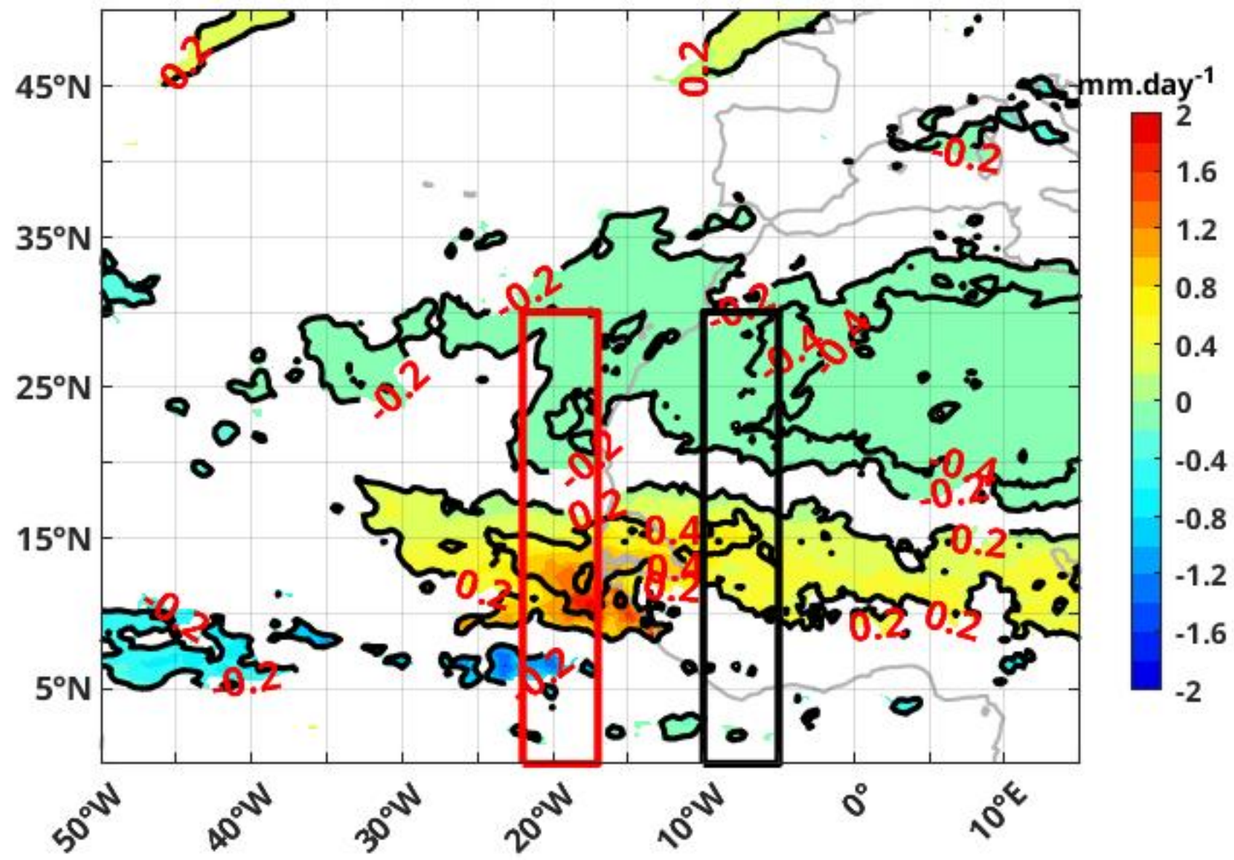

Figure 8.

a) JAS mean ∇.HT / HTx

b) JAS anomaly ∇.HT / HTx

c) JAS mean ∇.HT / HTx

d) JAS anomaly ∇.HT / HTx

Level (hPa)

400 500 600 700 800 900

JAS mean PPT

JAS anomaly PPT

mm/day

5°N 10°N 15°N 20°N 25°N

10^{-5} kg.m^{-2}.s^{-1}

10^{-6} kg.m^{-2}.s^{-1}

Figure 9.

JAS mean dZ/dy & Z

b) JAS anom. dZ/dy & Z

c) JAS mean dZ/dy & Z

d) JAS anom. dZ/dy & Z

Level (hPa)

400
500
600
700
800
900
1000

6500
4500
2500
500

-1.2
-1.8
-2.4
-3

0°
5°N
10°N
15°N
20°N
25°N
30°N

10^{-5} -5 -4 -3 -2 -1 0 1 2 3 4 5

10^{-6} -4 -3.2 -2.4 -1.6 -0.8 0 0.8 1.6 2.4 3.2 4

Figure A1.

a) EOF2 (10 %) PPT CRU

b) EOF2 (11%) PPT ERA5

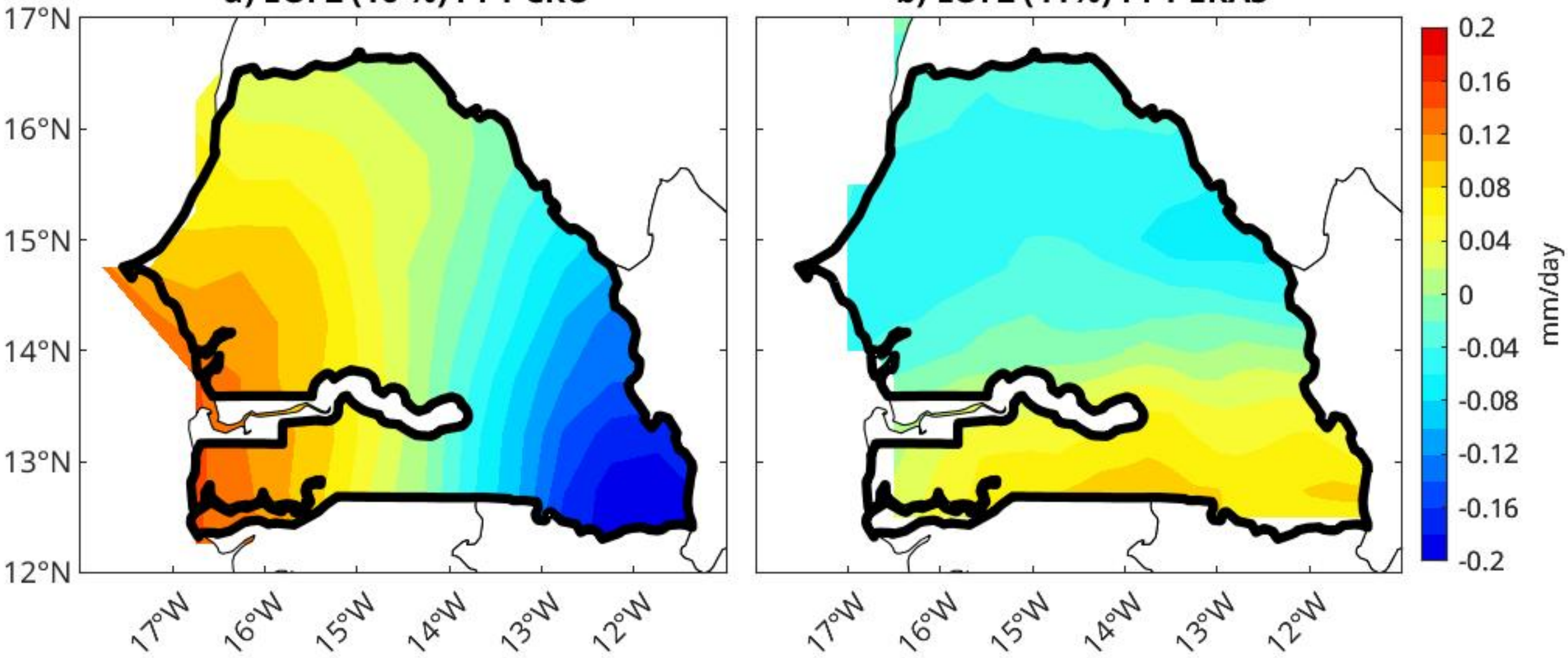

c) PC2 JAS PPT

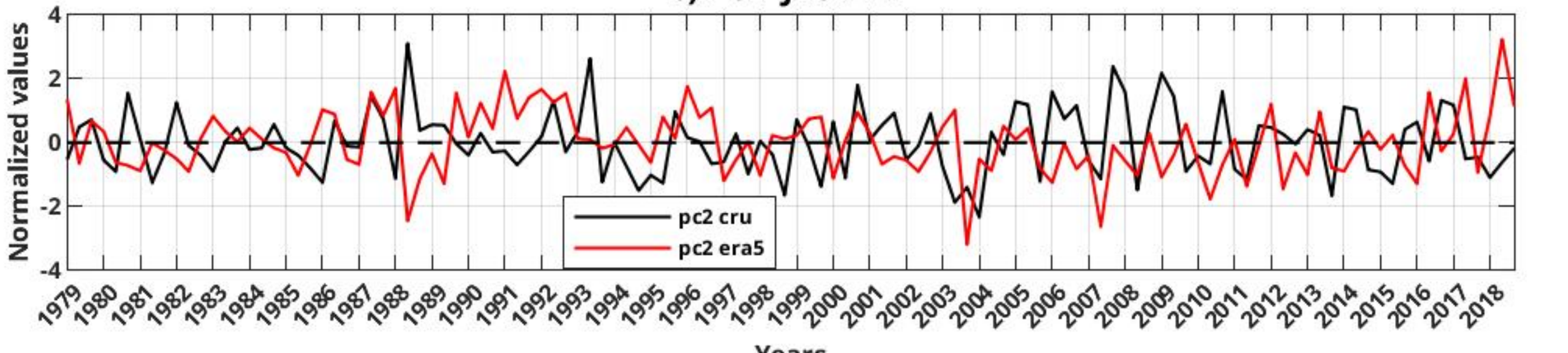

Figure A2.

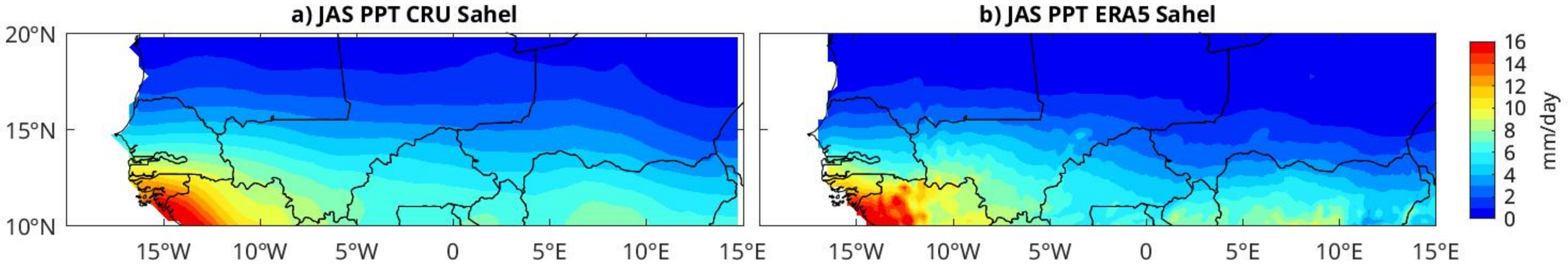
a) JAS PPT CRU Sahel
b) JAS PPT ERA5 Sahel
20°N
15°N
10°N
15°W
10°W
5°W
0
5°E
10°E
15°E
16
14
12
10
8
6
4
2
0
mm/day

Figure A3.

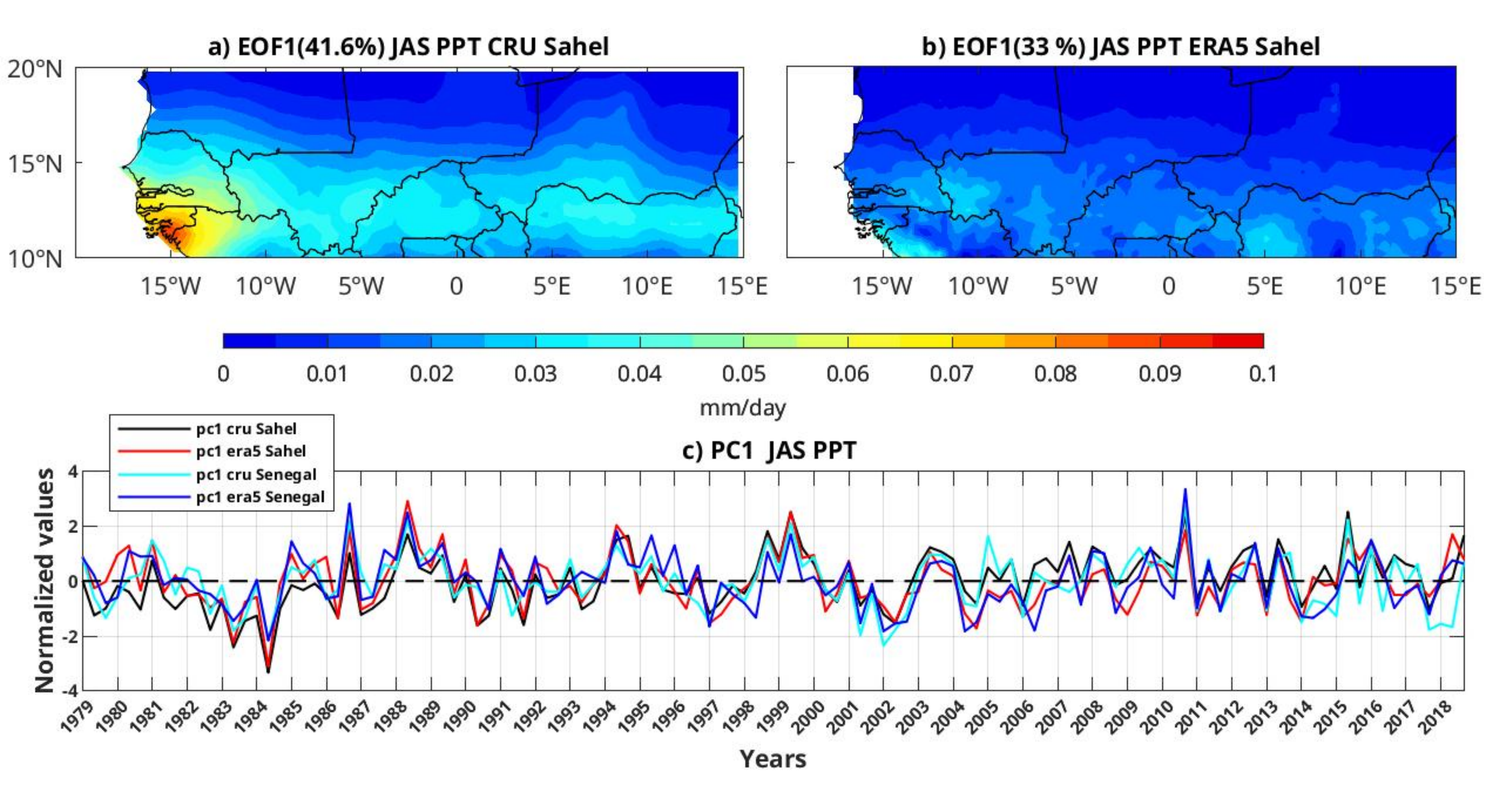
a) EOF1(41.6%) JAS PPT CRU Sahel
b) EOF1(33 %) JAS PPT ERA5 Sahel
20°N
15°N
10°N
15°W
10°W
5°W
0
5°E
10°E
15°E
0
0.01
0.02
0.03
0.04
0.05
0.06
0.07
0.08
0.09
0.1
mm/day
c) PC1 JAS PPT
pc1 cru Sahel
pc1 era5 Sahel
pc1 cru Senegal
pc1 era5 Senegal
Normalized values
4
2
0
-2
-4
1979
1980
1981
1982
1983
1984
1985
1986
1987
1988
1989
1990
1991
1992
1993
1994
1995
1996
1997
1998
1999
2000
2001
2002
2003
2004
2005
2006
2007
2008
2009
2010
2011
2012
2013
2014
2015
2016
2017
2018
Years